Journal of *Marine Science and Engineering*

MDPI

Review

A Review on the Recent Process of Lazy Wave Risers

Weidong Ruan [1,*], Chengcheng Zhou [1], Hongyu Yang [1], Zhi Wang [1], Bo Sun [1] and Yong Bai [2,*]

[1] Civil Engineering College, Zhejiang University of Technology, Hangzhou 310023, China; 201806080127@zjut.edu.cn (C.Z.); 13819124120@163.com (H.Y.); 221123060196@zjut.edu.cn (Z.W.); sunbo2017@zjut.edu.cn (B.S.)
[2] College of Civil Engineering and Architecture, Zhejiang University, Hangzhou 310058, China
* Correspondence: wdruan@zju.edu.cn (W.R.); baiyong@zju.edu.cn (Y.B.)

Abstract: Lazy wave risers (LWRs) are designed with equidistant buoyancy blocks attached in the lower half of the riser, allowing the riser to take on an arch shape under the buoyancy forces provided by buoyancy blocks. This arch configuration can provide flexibility to the LWR arrangement and effectively isolate the dynamic responses between the offshore floating structure and the riser's touchdown zone (TDZ). Its design and application aim to address the issues of dynamic response and fatigue damage that traditional steel catenary risers (SCRs) face in deep water and complex marine environments. Given that research on the LWRs in the field of ocean engineering is not sufficiently abundant, the structural characteristics, hydrodynamic loads, global responses, fatigue damage assessment, and structural optimization progress of LWRs are systematically reviewed in this paper to provide references for researchers in related fields. Among these topics, the global response of LWRs is the main point of this review. This section details the theoretical analysis and numerical modeling methods employed in the study of LWRs' global response, explores the research advancements in the vortex-induced vibration (VIV) related to LWRs, and discusses corresponding experimental studies. Finally, the installation, transfer, and repair processes of LWRs are investigated. Additionally, the importance of leveraging advanced technologies from other fields and combining them with current advanced algorithms is emphasized in efforts to assess fatigue damage and optimize the structures of LWRs, ultimately achieving complementary advantages.

Keywords: buoyancy block; fatigue damage; global response; LWR; VIV

Citation: Ruan, W.; Zhou, C.; Yang, H.; Wang, Z.; Sun, B.; Bai, Y. A Review on the Recent Process of Lazy Wave Risers. *J. Mar. Sci. Eng.* **2024**, *12*, 2000. https://doi.org/10.3390/jmse12112000

Academic Editor: Rodolfo T. Gonçalves

Received: 13 October 2024
Revised: 30 October 2024
Accepted: 4 November 2024
Published: 6 November 2024

1. Introduction

Deepwater oil and gas development has been recognized as a core growth area in the global petroleum industry. To enhance their core competitiveness, major oil companies and related research institutions in the world are increasingly investing financial and material resources in the pursuit of breakthroughs in deepwater technology. Therefore, deep-sea resource exploration and development technologies have become a research hotspot in international marine engineering [1]. As a crucial approach for transporting offshore oil and gas resources, subsea risers are employed to facilitate the transportation of oil/gas from the subsea wellhead to the upper floating structures at sea in actual offshore oil and gas extraction projects [2,3]. Subsea risers are not only the most complex and critical components in the subsea production system, but also the most vulnerable and susceptible marine structures.

When offshore oil and gas exploitation progresses from shallow water areas to deep water areas, traditional SCRs need to adapt to complex and harsh deep-sea environments. The SCRs are mainly subjected to high-temperature and high-pressure load inside and complex marine environmental load, seabed resistance, and severe coupling motions from the upper floating structure outside. These factors may lead to potential issues such as strength failure and fatigue damage in the risers [4–6]. Yang et al. point out that the intense floating production storage and offloading (FPSO) motion induced by harsh environments

may result in significantly amplified dynamic responses in traditional SCRs [7]. Therefore, traditional SCRs may not be suitable for the FPSO system in deepwater. To reduce the failure probability of subsea risers, Petrobras conducted research on various configurations of steel catenary risers focusing on extreme load conditions, vortex-induced vibrations, and wave-induced fatigue. They found that the LWR configuration is more suitable for deepwater applications in terms of structural performance and economic viability. The concept of LWR configuration was first proposed by Karunakaran et al. [8].

Compared with traditional SCRs, LWRs have better compliance, lower weight, and lower installation costs, exhibiting significant advantages in the future deepwater oil and gas exploitation [4,9]. As illustrated in Figure 1, LWRs utilize abundant buoyancy blocks bundled at equal intervals along the lower half of the riser [10]. The buoyancy provided by these blocks causes the riser to adopt an arch shape, effectively reducing the top tension of deepwater riser. This design can alleviate the coupling effects of floating structure motions on the riser's TDZ, thereby enhancing the fatigue life of the riser in the TDZ [11]. Buoyancy blocks are usually made from lightweight materials, such as synthetic foam or thin-walled air tanks, which have lower specific gravities than the seawater. As a result, the effective gravity of the buoyancy block becomes negative underwater, providing an upward lifting force.

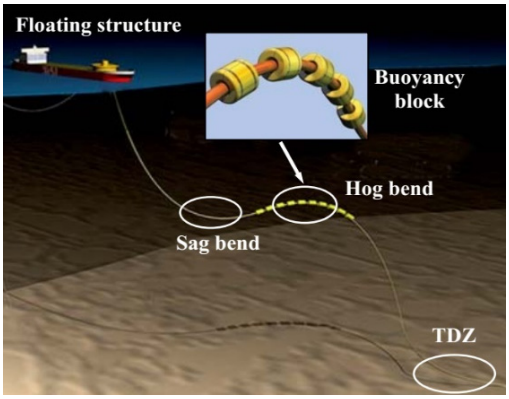

Figure 1. Deepwater LWR configuration [10].

On account of the introduction of buoyancy blocks, the mechanical properties of the riser segment bundled with equispaced buoyancy blocks are very different from those of the bare riser segment. Consequently, the LWRs are usually divided into three segments (suspended segment, buoyancy segment, and catenary segment, see Figure 2) for the global response study [12–17]. Meanwhile, some researchers divided the LWRs into four segments in order to distinguish the seabed resistance action [18–21]. As shown in Figure 2, there are four hazardous areas for the LWR: (1) hang-off location; (2) sag bend zone; (3) hog bend zone; (4) touchdown zone [16]. The hang-off location refers to the point where the riser is attached to the offshore production facility or platform. For steel lazy wave riser (SLWR), this connection is implemented by a flexible joint, which is treated as pinned [16,18,22,23]. For flexible LWR, the flexible riser is rigidly fixed to the floating structure with the bend stiffener constraint [22,24–26]. At this position, the riser is tension-controlled and able to withstand the significant dynamic loads applied. The hang-off angle should be designed within the range of 5 to 20 degrees to effectively prevent the risers from colliding with each other [27].

The sag bend zone refers to the downward bending section of the riser suspended segment due to the combined action of the riser self-weight, floating structure confinement, and lifting force of buoyancy segment. The requirements of fluid flow and structural strength in this zone should be guaranteed to prevent excessive bending stress throughout the design process. In addition, the sag bend zone should be designed as close to the seabed as possible, but the lowest point must avoid contact with the seabed [28]. For

the hog bend zone, it exhibits an arch form in the buoyancy segment with the buoyancy effect of abundant buoyancy blocks. The capability of the LWR to absorb the dynamic movements is suggested to be associated with this arch form height [29]. It follows that the rational distribution of buoyancy blocks on the buoyancy segment is a key factor in forming the ideal "wave shape" [30,31]. The height difference between the hog bend peak and sag bend trough should be controlled within certain limits to guarantee the fluid transport environment in the riser. On this account, Ruan et al. [10] proposed the new concept of deepwater LWR configuration based on multiple waveform serial arrangement (i.e., multiple LWR), which can greatly reduce this height difference to improve the fluid transport environment in the riser.

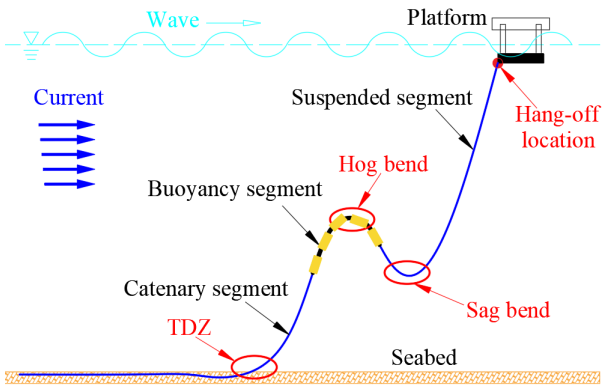

Figure 2. Schematic diagram of a LWR (adapted from [12]).

As illustrated in Figure 2, the TDZ of the riser is in the critical area where the catenary riser contacts with the seabed, and the touchdown point (TDP) is the point in the area where the catenary riser initially contacts with the seabed. Although the axial load of the riser in the TDZ is relatively small, the interaction between the riser flowline and seabed soil constantly occurs under the influence of the marine environmental loads and the floating body motion at the top, which makes this area a hot spot for riser fatigue analysis [32,33]. Ruan et al. [10] pointed out that compared to traditional catenary risers, a deepwater riser with lazy wave arrangement configuration can greatly attenuate the kinematic coupled response of the floating structure in the riser first sag bend section and effectively reduce the normal motion response of the LWR in the TDZ [10], which can effectively optimize the dynamic bending moment and antifatigue performance of the LWR in the TDZ. The results show that the maximum dynamic bending moments of the LWR in the TDZ decrease from 103.25 kN m to 64.86 kN m, with a decrease of up to 37.2%.

In recent years, scholars have conducted extensive and profound research on the global response of offshore risers, achieving remarkable outcomes. However, due to the complexities of deepwater environments and nonlinear boundary conditions, the analyses of offshore risers under complex deepwater conditions remain incomplete, particularly regarding the structural dynamic characteristics and motion responses of different deployment configurations. This study aims to summarize the primary achievements in the research on the global response of LWRs while identifying the current shortcomings and challenges. The review systematically organizes relevant research progress and emphasizes the contributions of various researchers in this field, to serve as a reference for future studies. In addition, key limitations in existing research, such as model accuracy, experimental validation, and multiple environmental factors, are presented. Furthermore, challenges in nonlinear behavior, fluid–dynamic interactions, and material property analysis are explored. This not only lays a foundation for a deeper understanding about the global response of LWRs, but also offers suggestions for subsequent research.

2. Hydrodynamic

The marine environment is a factor critical to the design and analysis of offshore risers and can cause multiple failure modes such as tensile failure, compression buckling, excessive bending, fatigue failure, and on-bottom instability.

2.1. Classification of Hydrodynamic Loads

The hydrodynamic loads caused by a marine environment can be divided into the following categories: (1) wave loads; (2) current loads. Waves are one of the most fundamental and significant hydrodynamic phenomena in the ocean. Wave loads include linear wave load, nonlinear wave load, and random wave load. Waves exert forces (such as drag force, inertial force, and buoyancy variations) on structures through the periodic motion of water particles. These forces have a significant impact on the motion and loading state of offshore riser systems. When calculating the wave forces on offshore risers, both inertial and viscous forces are important, which are often calculated by Morison equation [34]. Many experimental studies have provided the drag and inertia coefficients adopted in the Morison equation [35,36].

Currents are the steady water movement in the ocean and can be broadly categorized as tidal currents, wind-driven currents, ocean circulation, boundary currents including loop and eddy currents, and currents caused by internal waves and solitons. Currents are closely related to the density distribution and the flow into or out of an area, which is a function of the local topography and oceanography [34] (Figure 3a). For shallow water, since currents are frequently driven by tides, velocity–depth profiles can provide an adequate description; for deep water, both the velocity and direction of the currents change with the water depth, and are very complex to accurately describe (Figure 3b). The effects of currents on offshore riser systems are primarily manifested as constant drag forces and potential additional mass forces [6,29,37,38]. In addition, when ocean currents pass over offshore risers, a periodic vortex will be generated in the wake of the riser, and the periodic fluid force generated by the vortex falling off will stimulate the in-line flow (IF) and cross-flow (CF), and offshore risers will vibrate at the same time. This phenomenon is called vortex-induced vibration (VIV) due to ocean currents [6,29,37–39].

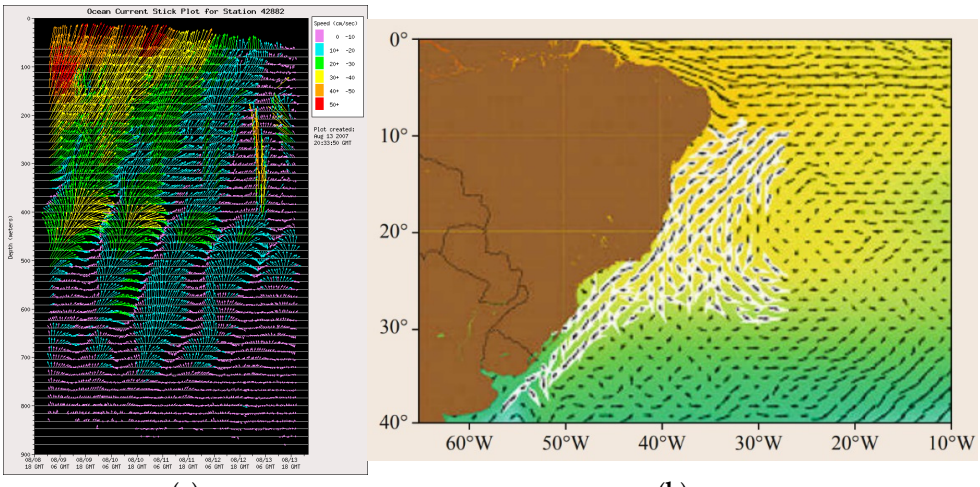

(**a**) (**b**)

Figure 3. Manifestation methods of ocean currents [34]. (**a**) Currents in the northern gulf of Mexico. (**b**) Brazil current as represented by the Mariano Global Surface Velocity Analysis.

Additionally, the waves and currents interaction (WCI) will further increase the complexity of the dynamic response of offshore riser systems [29,34]. Unlike the aforementioned, Yin et al. [27] divides the hydrodynamic loads acting on the LWRs into wave frequency loads, vortex-induced vibration due to currents, vortex-induced vibration due to vessel motion, loads due to internal flow, and low-frequency loads. The wave frequency loads

can further be divided into wave loads acting on the riser and wave frequency vessel motion-induced vibration according to the position of wave action. For the latter, when the LWR is subjected to vessel motion (such as heave motion), the sag bend and hog bend will move relative to the surrounding water. Consequently, the relative motion and velocity may cause the riser to experience vibrations similar to the VIV in oscillating flows.

2.2. Solution of Hydrodynamic Loads

2.2.1. Wave Theory

In a marine environment, fluid behaves with viscous characteristics, and at the same time, there is surface tension on the fluid surface. These factors have a certain impact on the wave movement. Because the effects of fluid viscosity and surface tension are related to wave frequency, these effects are negligible in the wave frequency bands that are generally important for offshore engineering. Therefore, it is assumed that the fluid is an ideal fluid, and only the influence of gravity is considered, i.e., the fluid motion is irrotational [40]. Any wave can be determined by wave height (or wave amplitude), wavelength (or wave period), and water depth, and the movement of water particles can be determined according to different wave theories. The velocity potential $\Phi(x, y, z, t)$ for an ideal fluid should satisfy Laplace equation [41]:

$$\nabla^2\Phi(x,y,z,t) = \frac{\partial^2\Phi}{\partial x^2} + \frac{\partial^2\Phi}{\partial y^2} + \frac{\partial^2\Phi}{\partial z^2} = 0 \tag{1}$$

where x, y, and z denote the coordinates of any point in space; t is the time. In order to solve the ideal fluid velocity potential expression, the following boundary conditions can be determined:

(1) Wave surface condition ($z = \xi$): the free surface pressure must be equal to the atmospheric pressure (regardless of the surface tension). By applying the Bayesian equation to the free surface of the wave, it can be obtained:

$$\frac{\partial\Phi}{\partial t} + \frac{1}{2}\left[\left(\frac{\partial\Phi}{\partial x}\right)^2 + \left(\frac{\partial\Phi}{\partial y}\right)^2 + \left(\frac{\partial\Phi}{\partial z}\right)^2\right]^2 + g\xi\Big|_{z=\xi} = 0 \tag{2}$$

where g is the acceleration of gravity. Meanwhile, the kinematic boundary conditions are satisfied, that is, the water particles on the free surface always remain on the free surface:

$$\frac{\partial\xi}{\partial t} + \frac{\partial\Phi}{\partial x}\frac{\partial\xi}{\partial x} + \frac{\partial\Phi}{\partial y}\frac{\partial\xi}{\partial y} - \frac{\partial\Phi}{\partial z}\Big|_{z=\xi} = 0 \tag{3}$$

(2) Bottom boundary conditions ($z = -d$): the vertical velocity is zero at the horizontal seabed:

$$\frac{\partial\Phi}{\partial z}\Big|_{z=-d} = 0 \tag{4}$$

Since water particles cannot pass through the seabed boundary, they can only move along the tangential direction of the seabed boundary, that is, the normal velocity of water particle perpendicular to the seabed boundary is zero.

$$\frac{\partial\Phi}{\partial n}\Big|_{z=-d} = 0 \tag{5}$$

(3) Condition at infinity: $\Phi(x, y, z, t)$ and $\xi(x, y, z, t)$ remain bounded, sometimes even requiring that both Φ and ξ and their derivatives approach zero.

2.2.2. Current Theory

Since the periodicity of ocean currents is in the order of several months, relative to the water particle velocity induced by waves, it is relatively slow to change over time. Hence, it can be considered that the velocity and direction of ocean currents remain unchanged over time in a given sea state, that is, a current is regarded as a steady flow. Of course, the velocity and direction of ocean currents change at different depths. In practical engineering design, engineers generally adopt "current profile" once in a decade and in a hundred years to carry out engineering design for offshore risers [42,43]. If a detailed profile of the current velocity is lacking, the power function rule can be employed to simulate the current velocity v_c at the depth z [44]:

$$v_c = v_b + (v_s - v_b) \cdot [(z - z_b)/(z_s - z_b)]^{1/n} \tag{6}$$

where v_s and v_b represent the surface velocity and seabed velocity, respectively; z_b and z_s donate the surface vertical coordinate and seabed vertical coordinate, respectively, and n is the exponential coefficient. The influence of ocean currents on offshore structures, especially deepwater structures, is very large and its analysis will be more complicated.

2.2.3. Hydrodynamic Load Calculation

Since the diameter of the offshore riser is much less than the incident wavelength, the structure itself has little influence on the wave motion, and the wave effect on the offshore riser mainly contains viscous effect and added mass effect. The Morrison equation proposed by Morison et al. [45] is generally adopted to calculate the wave loads. Morison et al. [45] pointed out that the wave loads acting on the offshore riser per unit length in water can be regarded as the linear superposition of two kinds of hydrodynamic loads: (1) drag force, caused by the water particle velocity when the seawater flows through the cylinder; (2) inertial force, caused by the water particle acceleration. Because ocean currents are generally treated to be steady currents, the hydrodynamic load caused by ocean currents is mainly manifested as drag force. It is necessary to linearly superposition the water particle velocity caused by the wave and current first, and then to calculate the total drag force acting on the offshore riser.

Because of the catenary configuration of the LWR, the calculation of hydrodynamic loads on the inclined cylinder should be considered, which is similar to the calculation of hydrodynamic loads on the vertical cylinder. Considering that the water particle velocity and acceleration of the inclined cylinder are generally not in the same spatial plane, the corresponding water particle velocity and acceleration are generally described in vector form, so as to calculate the hydrodynamic loads acting on the inclined cylinder. The expression of Morison equation in vector form for the LWR is as follows [46]:

$$\boldsymbol{f} = \rho_w \frac{\pi D^2}{4} \dot{\boldsymbol{v}} + C_a \rho_w \frac{\pi D^2}{4} (\dot{\boldsymbol{v}}_{\boldsymbol{n}} - \ddot{\boldsymbol{r}}_{\boldsymbol{n}}) + \frac{1}{2} C_d \rho_w D \, (\boldsymbol{v}_{\boldsymbol{n}} - \dot{\boldsymbol{r}}_{\boldsymbol{n}}) |\boldsymbol{v}_{\boldsymbol{n}} - \dot{\boldsymbol{r}}_{\boldsymbol{n}}| + C_{a\,t} \rho_w \frac{\pi D^2}{4} (\dot{\boldsymbol{v}}_{\boldsymbol{t}} - \ddot{\boldsymbol{r}}_{\boldsymbol{t}}) + \frac{1}{2} \pi C_{d\,t} \rho_w D \, (\boldsymbol{v}_{\boldsymbol{t}} - \dot{\boldsymbol{r}}_{\boldsymbol{t}}) |\boldsymbol{v}_{\boldsymbol{t}} - \dot{\boldsymbol{r}}_{\boldsymbol{t}}| \tag{7}$$

where ρ_w and D represent the sea density and riser's external diameter, respectively; $\dot{\boldsymbol{r}}$ and $\ddot{\boldsymbol{r}}$ are the riser moving velocity and acceleration vectors, where the subscripts "n" and "t" represent the riser's normal direction and tangential direction, respectively; $\boldsymbol{v}$ and $\dot{\boldsymbol{v}}$ denote the water particle velocity and acceleration vectors, where the meaning for the subscripts "n" and "t" are the same with riser velocity and acceleration vectors; C_d and C_a are the normal drag coefficient and added mass coefficient, meanwhile C_{dt} and C_{at} are the tangential drag coefficient and added mass coefficient.

3. Global Response of LWRs

Most researchers tend to carry out theoretical research and numerical simulation on the global response of LWRs because it is too time-consuming and costly to carry out experimental research on LWRs. The introduction of buoyancy blocks results in significant nonlinearity in the lazy wave configuration, and this configuration is notably affected by changes in the buoyancy blocks. Therefore, most scholars prefer to conduct large deforma-

tion nonlinear analyses and studies on the global response of LWRs [21,47,48]. OrcaFlex (version 11.4) is a widely applied dynamic simulation software in marine engineering and ship design, particularly for analyzing the dynamic behavior of marine structures, such as subsea pipelines, floating platforms, and offshore risers.

Based on the lumped mass method (LMM), this software allows for the setting of different boundary conditions, environmental conditions, and loading scenarios to adapt to various practical applications [9,13,49]. It also possesses powerful modeling capabilities that enable engineers to highly customize models based on specific requirements. Hu et al. [9] established OrcaFlex numerical models for the catenary riser and LWR to investigate how the response characteristics of offshore risers impact the stability and safety of the entire Offshore Compressed Air Energy Storage (OCAES) system (Figure 4). The results indicated that the structure of the LWR is more complex than the catenary riser; nevertheless, the former presents better response performance.

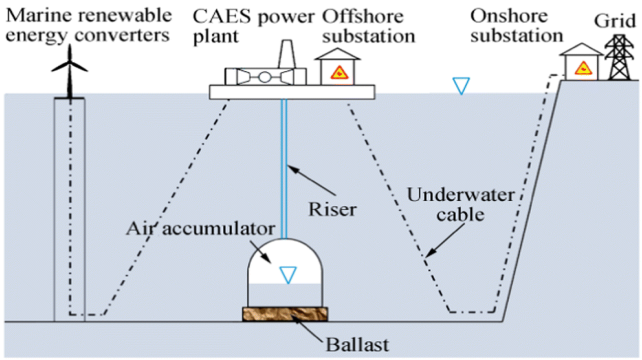

Figure 4. Typical configuration of an OCAES system [9].

3.1. Mathematical Model and Software Tools

The modeling of LWRs initially focused on two-dimensional (2D) models. With the improvement of computer computing power, there has been a gradual transition to three-dimensional (3D) models.

3.1.1. Two-Dimensional Model of LWRs

Early simulation software and insufficient computational power of computers hindered the ability to simulate 3D models of a LWR, leading to a significant computational burden. As a result, researchers primarily focused on developing 2D models for LWRs, accompanied by a series of simplifications and assumptions. For instance, the axial deformation and twisting behavior of the riser are often neglected [14,18,19]. Additionally, for the convenience of numerical modeling and mechanical analysis, the buoyancy segment of the LWR is simplified into a uniform pipe structure with constant inner and outer diameters based on the equivalence principles of hydrodynamic loads and buoyancy loads. Furthermore, during the global response analysis of the LWRs, it is usually necessary to consider the pipe–soil interaction. Therefore, the seabed in contact with the riser is generally assumed to be horizontal [15,17–19]. A such, most studies have treated the seabed as a horizontal and elastic foundation [13,14,18,50], typically modeled by the Winkler foundation model to simulate the normal seabed resistance loads.

In consideration of the boundary layer effects in the riser's TDZ and the buoyancy effects of the buoyancy segment, the LWR can be divided into several segments to carry out the analyses for 2D planar LWR models [13,14,18]. Compared to traditional small deformation beam theory or catenary theory, nonlinear large deformation beam theory has significant advantages in simulating rapid changes in the angle of the riser, making it more suitable for the mechanical analysis of deepwater risers with large deformations [51,52]. Wang et al. [18] employed nonlinear large deformation beam theory and small deformation beam theory to model the suspended segment (including the lower section, buoyancy

section, and upper section) and the flowline segment, respectively (Figure 5). The effects of the pipe–soil interaction, the bending stiffness of the riser, and the large deformation characteristics of the suspended segment were accounted for in this model. Under given boundary conditions, the governing equations were derived according to the finite difference method, and the numerical solution was obtained. Equation (8) presents the governing equation for the flowline segment based on small deformation beam theory, while Equations (9) and (10) represent the governing equations for the suspended segment based on nonlinear large deformation beam theory.

$$EI_r \frac{d^4 y_2}{dx^4} - T_2 \frac{d^2 y_2}{dx^2} + \mu y_2 + w_r = 0 \tag{8}$$

$$EI_r \frac{d^3 \theta}{ds^3} - T \frac{d\theta}{ds} + w_r cos\theta = 0 \tag{9}$$

$$\frac{dT}{ds} = w_r sin\theta \tag{10}$$

where EIr denotes the bending stiffness of the bare riser; T is the riser's axial tension; T_2 represents the unknown constant axial tension at the TDP; w is the riser's apparent weight in the water per unit length. More detailed information about symbols can be seen in [18]. When calculating the mechanical analyses for the buoyancy section with Equations (9) and (10), the corresponding bending stiffness and apparent weight should be updated.

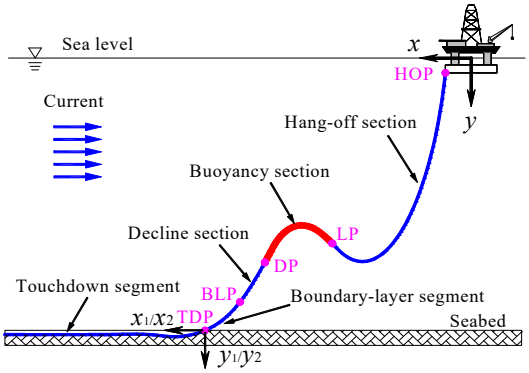

Figure 5. SLWR configuration [14].

However, this numerical model has a limitation issue, i.e., the length of the lower section is set as a known condition, which is hard to acquire through on-site measurements in actual engineering. Since the hang-off angle of the LWR can be obtained, some researchers took it as a known condition, instead of the length for the lower section. Then, Ruan et al. [14] proposed an efficient method to predict the accurate static stress range of deepwater SLWRs under the coupling effects of vessel slow drift motion and currents. The boundary layer effect in the riser's TDZ was well considered in this study, setting the riser segment close to the seabed as the individual boundary layer segment (Figure 5) and performing mechanical analysis according to small deformation beam theory. In contrast, catenary theory was adopted to calculate other sections of the suspended segment (including the hang-off section, buoyancy section, and decline section). This approach can effectively guarantee the continuity of the bending moment and shear force at the riser's TDP. It can be observed that the maximum axial stress range of the SCR occurs in the TDZ, reaching up to 112 MPa, which is 26% larger than that of the SLWR.

Unlike the solution of segmenting the LWR, Trapper [32] proposed a feasible numerical method for the LWR static configuration analysis. This method treated the entire riser as a continuous segment and modeled it according to nonlinear large deformation beam theory (Figure 6). Since the entire riser was considered as a continuous segment to conduct analysis,

the need to solve the governing equations for each segment separately was eliminated, and the boundary continuity between each segment also did not need to be considered. The model can accommodate additional loads, constraints, or boundary conditions flexibly. Compared to segmenting the model, the continuous riser model can significantly reduce the complexity of the governing equations. Based on the principle of minimum potential energy, the configuration equation for the LWR in equilibrium is as follows:

$$U_{tot} = \frac{1}{2}\int_L EI\kappa(s)^2 ds + \frac{1}{2}\int_{L_s} k_s e(s)^2 ds - \int_L w_g y(s) ds - \int_{L_b} w_b y(s) ds - \int_L f_x x(s) ds - \int_L f_y y(s) ds - P_0 x(L) \quad (11)$$

where E and I represent the riser's Young's modulus and cross-sectional inertia moment, respectively; κ and $e(s)$ denote the riser's curvature and embedment into the seabed, respectively; L_s and L_b are the section length in contact with soil and buoyancy section length, respectively. The right terms in Equation (11) represent the bending elastic energy stored in a deformed riser, the elastic energy stored in the deformation of elastic seabed, the potential energy of the riser's submerged self-weight, and the potential energy of submerged self-weight for buoyancy blocks averaged over the section length, respectively.

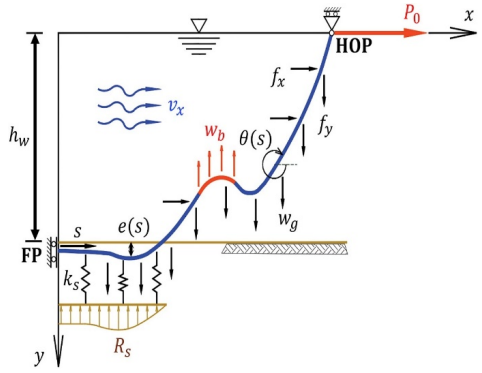

Figure 6. LWR scheme: geometry, loads, boundary conditions, and coordinate systems [32].

When investigating the global response of LWRs, the effect of the internal flow in the riser was generally ignored in numerical models. However, the internal flow can reduce the structural stiffness provided by the negative damping [53] and induce additional large riser displacements [54]. Therefore, Ruan et al. [12] established a dynamic model for the global response of LWRs under imposed top-end excitations and internal flow according to the elastic slender rod theory. The research found that the relative position and length of the buoyancy section can significantly impact the maximum bending moments in the sag bend zone, hog bend zone and TDZ, and the top tension at the hang-off point. However, this study did not specifically focus on the effects of the internal flow on the global dynamic response of the LWR. The elastic rod theory primarily contains a motion governing equation and a stretching constraint equation. By applying Galerkin's method for discretization and the tensor summation algorithm, a set of nonlinear ordinary differential equations in the time domain can be obtained:

$$\gamma_{ikm} M_{njm} \ddot{u}_{kj} - 2\rho_i A_i U \zeta_{ik} \dot{u}_{kn} + \alpha_{ikm} EI_m u_{kn} + \beta_{ikm} \overline{\lambda}_m u_{kn} = \mu_{im} q_{mn} + f_{in} \quad (12)$$

$$\frac{1}{2}\beta_{ikm} u_{in} u_{kn} - \frac{1}{2}\tau_m - \eta_{mn} \frac{\overline{\lambda}_n - (p_{on} A_o - p_{in} A_i) + \rho_i A_i U^2}{EA_n} = 0 \quad (13)$$

where i and k run from 1 to 4; j, m, and n run from 1 to 3. Detailed information about tensor expressions can be seen in [12].

Subsequently, Wang et al. [47] considered the effects of currents and internal flow and proposed a 2D nonlinear dynamic model for deepwater LWRs under normal and tangential top excitations based on Euler–Bernoulli beam theory and Keller Box finite difference approach. Through parameter analysis, it was found that the floating structure motion,

internal fluid, and ocean current loads significantly affect the mechanical properties of LWRs. Jeong et al. [55] established a dynamic response analysis program for the LWRs accounting for environmental loads and slug flow. The dynamic responses of the LWRs under critical conditions with and without slug flow were analyzed and compared to provide a quantitative comparison of the effects of slug flow on the LWRs. As displayed in Figure 7, Cabrera-Miranda and Paik [56] modeled the LWR as an Euler–Bernoulli beam to investigate the nonlinear planar vibrations of LWRs excited by slug flow, in which the internal fluid was treated as a plug flow with time-space-varying mass in the form of a rectangular pulse train. The partial differential governing equations for the LWR planar motion in this model are as follows:

$$m\frac{\partial u}{\partial t} - (m+M)\frac{\partial \phi}{\partial t}v + \frac{MU}{1+e}\left(\frac{\partial U}{\partial s} - \Omega_3 v\right) = \frac{\partial T_e}{\partial s} - S_n\Omega_3 - (w_0+Mg)\sin\phi - \frac{1}{2}\pi\rho D_0 C_{dt}u|u|\sqrt{1+e} \quad (14)$$

$$(m+m_a+M)\frac{\partial v}{\partial t} + m\frac{\partial \phi}{\partial t}u + \frac{MU}{1+e}\left(\frac{\partial v}{\partial s} + \Omega_3 U\right) = \frac{\partial S_n}{\partial s} + \Omega_3 T_e - (w_0+Mg)\cos\phi - \frac{1}{2}\rho D_0 C_d v|v|\sqrt{1+e} \quad (15)$$

$$\frac{1}{EA_p}\frac{\partial T_e}{\partial t} = \frac{\partial u}{\partial s} - \Omega_3 v \quad (16)$$

$$(1+e)\frac{\partial \phi}{\partial t} = \frac{\partial v}{\partial s} + \Omega_3 v \quad (17)$$

$$EI\frac{\partial \Omega_3}{\partial s} + S_n(1+e)^3 = 0 \quad (18)$$

$$\frac{\partial \phi}{\partial s} - \Omega_3 = 0 \quad (19)$$

where s denotes the local curvilinear Lagrangian coordinate related to the unstretched riser of length L; M represents the fluid mass in the riser. More detailed symbol explanations can be seen in [56].

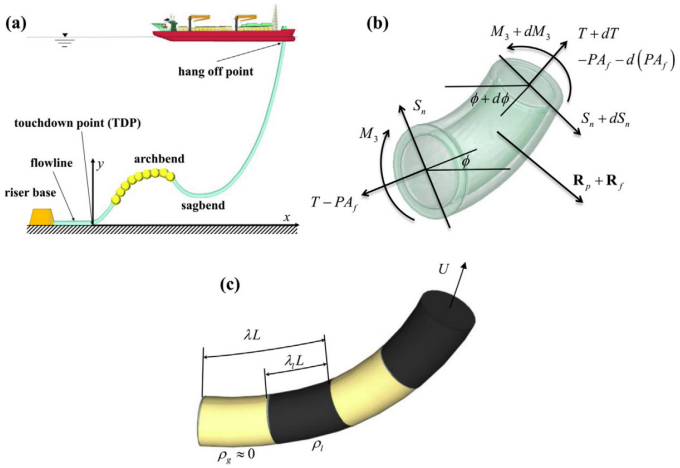

Figure 7. Riser subjected to two-phase flow-induced vibrations [56]. (**a**) sketch of steel lazy wave riser, (**b**) in-plane balance of forces and moments acting on a pipe conveying fluid after elongation and (**c**) internal fluid with time-space-varying mass in the form of a rectangular pulse train.

The global response analysis method for the LWRs has evolved from the initial small deformation beam theory and catenary theory to nonlinear large deformation beam theory, resulting in a mature theoretical system. Meanwhile, some researchers are still exploring new theoretical frameworks and progressively developing them. The theoretical system in other fields has been applied to the field of ocean engineering, and some achievements have been achieved, such as the absolute nodal coordinate formulation (ANCF) method [57]. The ANCF method is a dynamic analysis approach widely used in mechanical engineering,

multi-body dynamics, and aerospace engineering in recent years, which can solve the problem of flexible bodies with large deformation and large rotation.

Furthermore, ANCF can alleviate inherent numerical problems associated with nonlinear dynamic analysis, such as non-physical oscillations and peak values. Therefore, the ANCF method is regarded as a promising theoretical approach for the dynamics analysis of flexible structures like risers and cables in offshore operations. Based on the ANCF and continuum mechanics theory, Zhang et al. [57] utilized the finite element method to establish a mechanical analysis model to investigate the static and dynamic responses of LWRs, extending the ANCF method to the field of marine engineering. The results obtained from the ANCF approach were larger than those by the LMM, and the maximum error reached about 6.65%. Wang et al. [58] applied the ANCF method to the simulation of flexible structures in marine operation and developed internal code MiNos using MATLAB program. Compared to OrcaFlex software, MiNos demonstrated a reduction in significant bending moment peaks due to the superior continuity of the ANCF elements.

3.1.2. Three-Dimensional Model of LWRs

Compared to 2D models of LWRs, 3D models can more accurately represent the shape and structure response of a riser, including its configuration, inclination angles, and connection points, thus providing a more comprehensive reflection of its actual design. Additionally, 3D models can account for loads from different directions, such as waves and currents, allowing for better simulation and analysis of a riser's dynamic response in a complex marine environment. Li et al. [48] employed the vector form intrinsic finite element (VFIFE) method to establish a physical model of the LWR and analyze its nonlinear behavior in 3D space. Differently from traditional mathematical models, the VFIFE method, based on vector mechanics theory and numerical computation, does not require the integrated stiffness matrix and the iterative solution for the governing equations, so it can effectively solve structural problems flexibly. As depicted in Figure 8, the initial riser is assumed to be an oblique straight line meshed into N segments by $N + 1$ particles. Meanwhile, the gravity, buoyancy forces, and hydrodynamic loads are loaded on the riser with ramp function to eliminate transient response and reduce the time to obtain steady-state response. Considering the effect of the structural damping, the governing equations for the particle can be expressed:

$$m_j \frac{d^2}{dt^2} \begin{bmatrix} x_j \\ y_j \\ z_j \end{bmatrix} = \begin{bmatrix} f_{jx}^{exi} \\ f_{jy}^{exi} \\ f_{jz}^{exi} \end{bmatrix} + \begin{bmatrix} f_{jx}^{int} \\ f_{jy}^{int} \\ f_{jz}^{int} \end{bmatrix} + \begin{bmatrix} f_{jx}^{dmp} \\ f_{jy}^{dmp} \\ f_{jz}^{dmp} \end{bmatrix} \tag{20}$$

$$\begin{bmatrix} I_{xx} & 0 & 0 \\ 0 & I_{yy} & 0 \\ 0 & 0 & I_{zz} \end{bmatrix} \frac{d^2}{dt^2} \begin{bmatrix} \theta_{jx} \\ \theta_{jy} \\ \theta_{jz} \end{bmatrix} = \begin{bmatrix} m_{jx}^{exi} \\ m_{jy}^{exi} \\ m_{jz}^{exi} \end{bmatrix} + \begin{bmatrix} m_{jx}^{int} \\ m_{jy}^{int} \\ m_{jz}^{int} \end{bmatrix} + \begin{bmatrix} m_{jx}^{dmp} \\ m_{jy}^{dmp} \\ m_{jz}^{dmp} \end{bmatrix} \tag{21}$$

where m_j denotes the mass of the particle j; the position vector $\boldsymbol{X}_j$ (x_j, y_j, z_j) in the particle motion formula and the direction vector $\boldsymbol{\theta}_j$ for the particle j are described by the global coordinates. More detailed symbol explanations can be seen in [48].

The above research adopts the uncoupled method to investigate the dynamic response of the riser system, which decouples the riser from the vessel movement and can reduce the dynamic top tension, TDZ stress, and fatigue damage [59–62]. This decoupled method does not consume excessive computational resources and is time-efficient. However, this method has certain limitations in the analysis of floating offshore systems: it separates the analysis of vessel motion from the load effects of mooring lines and risers into two steps, ignoring the interactions between them [63,64].

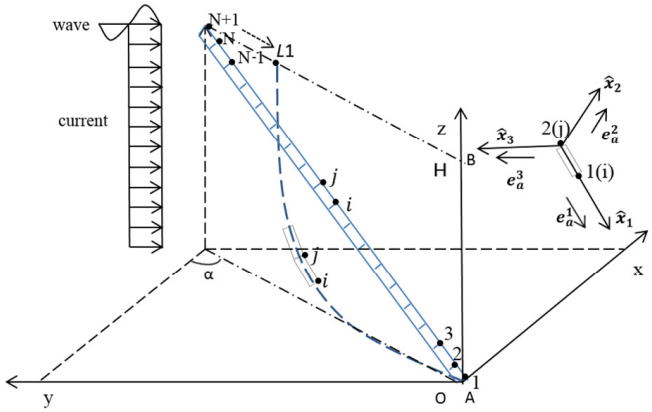

Figure 8. Riser model based on VFIFE method [48].

To comprehensively consider the interactions among various components in the system and improve the accuracy and reliability of structural analyses, coupled methods were developed. Ormberg and Larsen [63] conducted numerical simulations using both uncoupled and coupled methods, and they pointed out that the consistency of the model verification results with the coupled method was higher compared to the decoupled method. Then, Kim and Kim [15] developed the time-domain hull/mooring/riser fully coupled dynamic simulation program CHARM3D to carry out coupled numerical analyses. The transmitted forces from the mooring lines and risers to the platform are given as follows:

$$\widetilde{F}_P = \widetilde{K}(\widetilde{T}\widetilde{u}_P - \widetilde{u}_I) + \widetilde{C}(\widetilde{T}\dot{\widetilde{u}}_P - \dot{\widetilde{u}}_I) \tag{22}$$

Then, the hull response equation can be added into the riser/mooring equations in the time domain:

$$\left(\widetilde{M} + \widetilde{M}_a(\infty)\right)\ddot{\widetilde{u}}_p + \int_0^\infty \widetilde{R}(t-\tau)\dot{\widetilde{u}}_p \mathrm{d}\tau + \widetilde{K}_H\widetilde{u}_p = \widetilde{F}_D + \widetilde{F}^{(1)} + \widetilde{F}^{(2)} + \widetilde{F}_p + \widetilde{F}_w + \widetilde{F}_c + \widetilde{F}_{WD} \tag{23}$$

where $\widetilde{K}$ and $\widetilde{C}$ are the stiffness and damping matrices for mooring lines at the connection point; $\widetilde{M}$ and $\widetilde{M}_\mathrm{a}$ are the mass and added mass matrix; $\widetilde{R}$ denotes the retardation function matrix. More detailed symbol explanations can be seen in [15].

By comparing the dynamic characteristics of the SCR and SLWR near TDZ, Kim and Kim [15] pointed out that the local dynamic buckling of the SCR near the TDZ will exacerbate the bending moment and bending stress responses in that area; in contrast, the LWR can effectively avoid local dynamic buckling near the TDZ due to its additional sag and hog bends, which can absorb the dynamic motion energy. In addition, the slender rod theory was employed in the CHARM3D program to carry out the static and dynamic analysis of mooring lines and risers. This theory was initially proposed by Nordgren [65] and Garrett [66]. Its major advantage lies in the fact that the motion governing equations are formulated directly in the global coordinate system and include all geometric nonlinearities, which can eliminate the cumbersome coordinate transformations between different coordinate systems and improve computing efficiency. Consequently, it has been widely applied in studies of static/dynamic response of marine slender rod structures [13,67–69]. Based on the initial slender rod theory, Paulling and Webster [70] improved and proposed a slender rod theory model with the assumption of small tensile deformations. To date, Texas A&M University has conducted extensive and systematic research on the slender rod theory and developed the fully coupled computation program CABLE 3D in Fortran to study the global coupled dynamic responses of floating production systems, anchor lines, and offshore risers [71–75].

Taking the effects of internal flow and seabed resistance into account, Cheng et al. [21] utilized 3D slender rod theory to investigate the dynamic performance of a LWR under vessel offsets and wave-current loads. This research indicated that when the LWR is

subjected only to wave and current loads, internal flow parameters such as density, velocity, and top pressure have a significant impact on the LWR dynamic behavior. Based on a 3D modified slender rod theory, Li et al. [76] and Ruan et al. [77] employed an extended Korteweg-de Vries equation to simulate internal solitary waves (ISW) to study the nonlinear dynamic response of a LWR subjected to vessel motions, surface waves, ocean currents, and ISW. They discovered that ISW can induce significant oscillatory displacements in both the horizontal and vertical directions of the LWR, which notably increases the possibility of riser collision and shear damage. Yu et al. [78] established a self-developed program to describe the dynamic behavior of the coupled platform-mooring-riser system. The configurations of two types of risers (SCR and LWR) under the combined excitation of ISW and random waves were well compared. The results demonstrated that compared to SCRs, LWRs consistently exhibit greater motion responses with time differences due to complex configurations.

In addition, Yu et al. [78] established a fully coupled analysis model of floating platform-mooring-risers (SCRs and SLWRs) under the effects of ISWs and random waves. Rigid body dynamics theory and LMM were adopted to simulate the responses of the floating platform and riser/mooring lines, respectively, achieving the coupling effect between them through semi-coupled analysis. As shown in Figure 9, the LMM was employed to simulate the riser/mooring line configuration:

$$\boldsymbol{R}_k = \sum_{i=1}^{3} r_{i,k}\boldsymbol{n}_i, k = 1, 2, \ldots, n \tag{24}$$

$$\boldsymbol{S}_{k+1/2} = \boldsymbol{R}_{k+1} - \boldsymbol{R}_k = \sum_{i=1}^{3} (r_{i,k+1} - r_{i,k})\boldsymbol{n}_i, k = 1, 2, \ldots, n-1 \tag{25}$$

$$l_{k+1/2} = |\boldsymbol{R}_{k+1} - \boldsymbol{R}_k| = \sqrt{\sum_{i=1}^{3} (r_{i,k+1} - r_{i,k})^2}, k = 1, 2, \ldots, n-1 \tag{26}$$

$$\boldsymbol{t}_{k+(1/2)} = \frac{\boldsymbol{S}_{k+(1/2)}}{\boldsymbol{l}_{k+(1/2)}} = \frac{\sum_{i=1}^{3} (\boldsymbol{r}_{i,k+1} - \boldsymbol{r}_{i,k})\boldsymbol{n}_i}{\sqrt{\sum_{i=1}^{3} (\boldsymbol{r}_{i,k+1} - \boldsymbol{r}_{i,k})^2}}, \boldsymbol{k} = 1, 2, \cdots, \boldsymbol{n}-1 \tag{27}$$

$$\boldsymbol{q}_k = \frac{\boldsymbol{R}_{k+1} - \boldsymbol{R}_{k-1}}{|\boldsymbol{R}_{k+1} - \boldsymbol{R}_{k-1}|} = \frac{\sum_{i=1}^{3} (\boldsymbol{r}_{i,k+1} - \boldsymbol{r}_{i,k-1})\boldsymbol{n}_i}{\sqrt{\sum_{i=1}^{3} (\boldsymbol{r}_{i,k+1} - \boldsymbol{r}_{i,k-1})^2}}, \boldsymbol{k} = 2, 3, \cdots, \boldsymbol{n}-1 \tag{28}$$

where $\boldsymbol{R}_k$ denotes the position vector of the kth lumped mass point; the segment vector pointing from $\boldsymbol{R}_k$ to $\boldsymbol{R}_{k+1}$ is denoted as $\boldsymbol{S}_{k+1/2}$, with its length defined as $l_{k+1/2}$; the tangent direction $\boldsymbol{q}_k$ at each node is approximated as the direction pointing between two adjacent nodes to calculate the hydrodynamic loads. More detailed symbol explanations can be seen in [78].

In summary, research on the global response of LWRs has gradually shifted from initial static response analyses to dynamic response analyses. Due to the complex dynamic loads (including wave loads, structural stiffness, and hydraulic resistance) acting on the LWRs, dynamic simulations are more effective and accurate compared to static simulations in reflecting real-world conditions. For this reason, design and validation techniques based on dynamic simulations have been actively researched in marine operations, which aligns with current and future research trends.

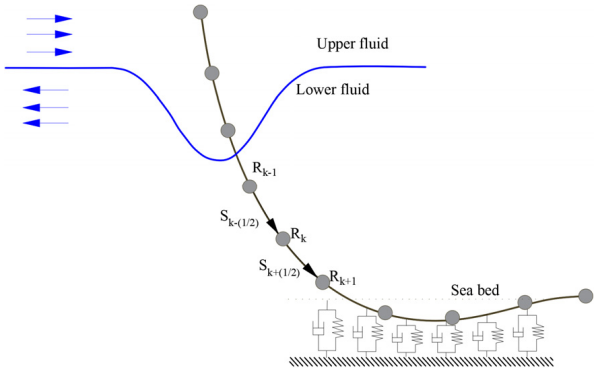

Figure 9. Discretization of riser/mooring based on the LMM [78].

3.2. Vortex-Induced Vibration

VIV could lead to the rapid accumulation of fatigue damage in risers and amplify the drag effects acting on the riser, which is induced by ocean currents and vessel motions. The occurrence and characteristics of the VIV are closely related to the Reynolds number. As the Reynolds number increases, the frequency and patterns of vortex shedding will change, which will affect the intensity and nature of the VIV. With low Reynolds numbers, vortex shedding usually presents a regular Karman vortex street pattern; however, with high Reynolds numbers, vortex shedding may become irregular, resulting in increased complexity and unpredictability of the VIV. Figure 10A showcases 3D vortex structures in the wake of a circular cylinder under different Reynolds number conditions [79]. These vortex structures include vortex loops and streamwise vortex pairs. With the increasing the Reynolds number, the vortex structures in the wake become more complex and unstable, exhibiting pronounced 3D characteristics [80]. Additionally, the flow field near the separation point on the cylinder varies across different Reynolds number regimes [81]. The period of vortex shedding is illustrated in Figure 10B. In this Figure, only the separatrices are shown, i.e., streamlines that leave or terminate at a saddle point.

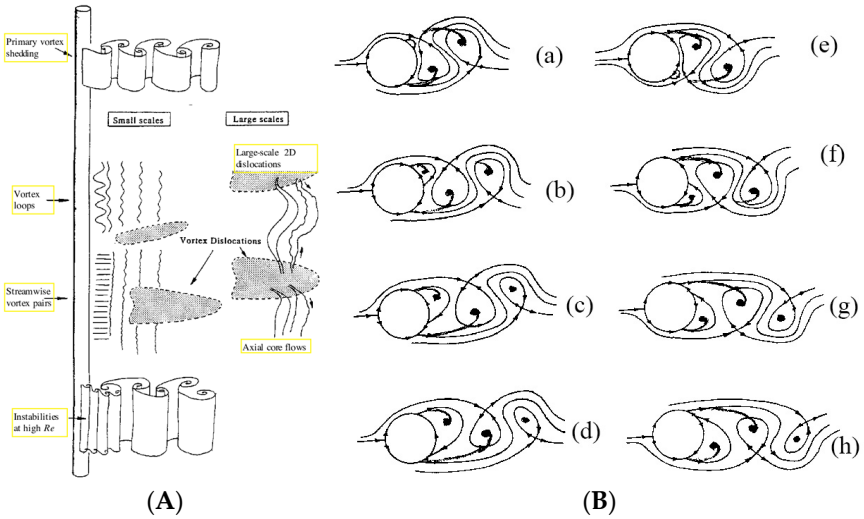

Figure 10. Vortex structures and vortex shedding period. (**A**) 3D features in the wake of a circular cylinder [79]. (**B**) Simplified model of vortex shedding period (**a**–**h**) [81].

In most cases, the time-varying and spatially varying ocean currents acting on the LWRs can be simplified to the steady current through a circular cross-section. When steady currents pass over offshore risers, periodic vortex will be generated in the wake of the riser, and offshore risers will vibrate at the same time, which is called VIV due to ocean currents [6,29,37–39]. However, rapidly time-varying currents and relative oscillations

caused by vessel motions may lead to oscillatory currents. Under the action of vessel motions, the LWRs will be subjected to time-varying oscillatory currents, which may generate vorticity and periodic vortex-induced force, and finally cause the vibration of offshore risers. This fluid–structure interaction is called VIV due to vessel motion [82,83].

Research on the riser VIV primarily involves the application of computational fluid dynamics (CFD) for numerical simulations of the cylinder by both domestic and foreign scholars. However, studies on the VIV response for the combined structures with the riser and staggered buoyancy blocks are still relatively scarce. Jang and Kim [84] employed CFD simulation to numerically model the VIV response of the SLWR combined structure with staggered buoyancy blocks and riser and solved the structural equations of motion through modal analysis. As illustrated in Figure 11, Constantinides and Zhang [85] adopted a combination of CFD technology and semi-empirical software analysis to investigate the global response of a deepwater LWR with staggered buoyancy blocks.

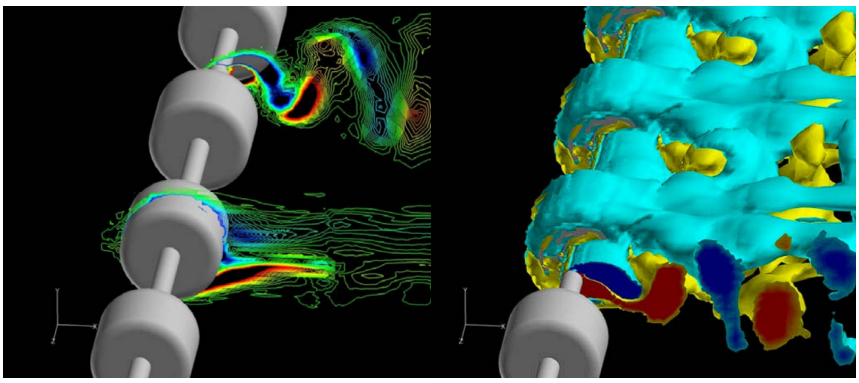

(**a**) (**b**)

Figure 11. CFD simulation of riser with staggered buoyancy blocks [85]. (**a**) Buoyancy module configuration illustrating flow over bare cylinder and buoyancy module. (**b**) Vortex structures over the buoyancy module area.

3.2.1. VIV Due to Vessel Motion

Due to the influence of vessel motion, the VIV response of the riser may become more complex. The vessel's roll and pitch motions would affect the formation and shedding patterns of vortices, subsequently altering the riser vibration characteristics [86]. Based on time-domain analysis method and the SIMA software workbench, Yin [82,83] simulated the VIV response of a full-scale LWR under the effect of vessel motion. This study constructed the total hydrodynamic loads in the CF direction:

$$F_{hydro,y} = \underbrace{\frac{1}{2}\rho D C_v |v_n|(j_3 \times v_n)\cos\phi_{exc}}_{vortex\ shedding} + \underbrace{\frac{1}{2}\rho D C_D |v_n| v_n}_{drag} + \underbrace{\frac{1}{4}\rho\pi C_M D^2 \dot{u}_n}_{water\ particle} - \underbrace{\frac{1}{4}\rho\pi(C_M - 1)D^2\ddot{x}_n}_{cylinder\ added\ mass} \quad (29)$$

where the first term on the right side of Equation (29) represents the oscillating lift force due to vortex shedding, and the three last terms make up the Morison equation. More detailed symbol explanations can be seen in [82,83].

Research found that vessel motion will induce a normal relative velocity that varies along the LWR, with the largest value occurring at the lower part of the upper catenary. It was also pointed out that the VIV response of the LWR is dominated by the bare riser section. Additionally, Yin [82,83] highlighted the limitations of the time-domain models: since these time-domain models are semi-empirical, input parameters need to be obtained through experiments. Future improvements for the LWR's VIV due to vessel motion are needed in the following areas:

1. Rigid model (staggered buoyancy arrangement) test in oscillatory flow;
2. Computational fluid mechanics simulations to investigate 3D effects;

3. Experimental techniques to measure the displacement responses;
4. Higher-order components included in the time-domain model;
5. The consideration of in-line forces.

3.2.2. VIV Due to Current

Both the bare riser and buoyancy blocks in the LWR may experience the VIV under the influence of ocean currents. However, when the VIV occurs, the hydrodynamic characteristics of buoyancy blocks and their influence on the hydrodynamics of the bare riser section still require further investigation. A large number of studies indicated that the coverage of buoyancy blocks plays a crucial role in the competitive excitation between the bare riser section and buoyancy regions [37,87,88]. If the flexible cylinders with a staggered buoyancy system are linear, the frequency components in response will be the same as those in excitation forces; if the system is nonlinear, excitation frequency components will include those in the excitation forces and additional frequencies [87]. These additional frequencies arise from the nonlinear interaction of the cylinder's response at the excitation frequency components.

Subsequently, Rao et al. [37] investigated the VIV excitation characteristics of the buoyancy section and bare section of the LWR under five staggered buoyancy configurations. The research found that under almost all velocity conditions, the excitation response of the bare region predominates in pipes with a buoyancy block length-to-diameter ratio of 3. Furthermore, there were generally two excitation frequencies presented in the spectrum of risers with staggered buoyancy blocks, with the higher frequency related to the bare region and the lower frequency related to the buoyancy section. However, in addition to these two excitation frequencies, a third excitation frequency was observed (Figure 12), which is an unexpected combination of the two excitation frequencies and may arise from the nonlinear effects of hydrodynamic damping mechanisms.

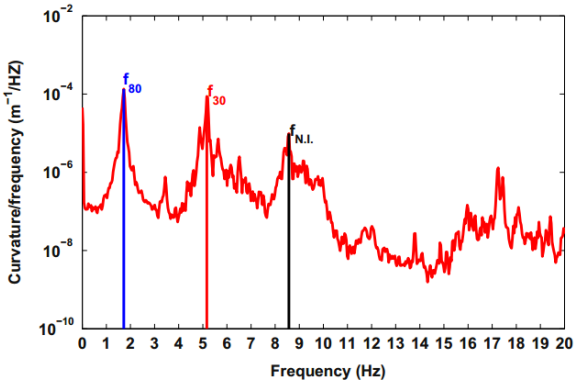

Figure 12. Schematic diagram of three frequencies [37].

To identify and compare the VIV responses in different regions, a frequency component identification method was proposed by Rao et al. [37]. The VIV excitations associated with 30 mm and 80 mm pipe diameters could be identified through the frequency components. The corresponding average VIV power can be computed numerically with Equations (30) and (31):

$$P_{30} = \int_L \frac{1}{T} \int_0^T c_{30} \dot{y}_{30}^2 dt dx \tag{30}$$

$$P_{80} = \int_L \frac{1}{T} \int_0^T c_{80} \dot{y}_{80}^2 dt dx \tag{31}$$

The reconstructed displacements y_{30} and y_{80}, and the damping c_{30} and c_{80} represent the corresponding values at fundamental excitation frequencies associated with 30 mm and 80 mm pipe diameters, respectively.

The forces induced on the risers by slug flows are intermittent, thus inducing excitations that may cause large oscillations on the suspended risers [89]. This internal flow-induced vibration can affect the VIV, and the two will interact, potentially causing resonance [90]. Bordalo and Morooka [89] established subroutines for internal flow forces to maintain a constant two-way dialog with the dynamic integrator of the pipeline movement simulator for solving the equations of motion for the riser (Figure 13). The research found that due to the influence of slug mass on the system's weight and inertia, the LWR oscillations induced by the VIV were altered in the presence of slugs. In the case of slug flow, intermittent mass distribution can lead to oscillatory motions in the suspended risers, thereby affecting the VIV response. Zhu et al. [91] investigated the VIV of a flexible LWR filled with various fluid media, including water and helium as typical examples of liquid and light gas, respectively. Similarly to [38], the VIV tests were conducted in the depth-averaged reduced velocity (Ur) range of 9.32–23.19 using non-intrusive optical measurement techniques with several high-speed cameras. The results indicated that when the internal fluid changed, both the excitation patterns and response amplitudes of the in-plane response were significantly adjusted, while the excitation patterns of the out-of-plane response showed no notable changes.

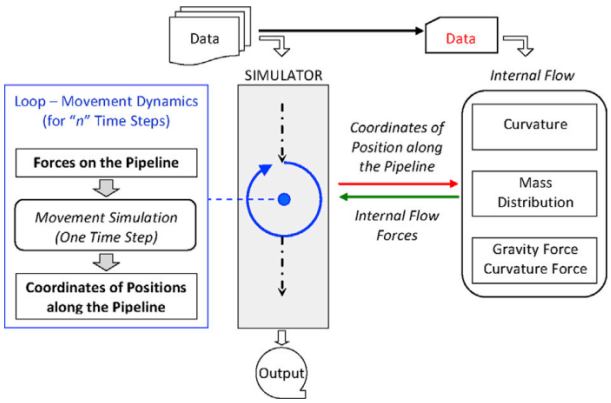

Figure 13. Interaction flowchart between pipeline simulator and internal flow subroutines [89].

3.3. Experiment

Due to the numerous assumptions commonly employed in numerical calculations, the results may be unreliable. To obtain accurate model results, the offshore engineering community tends to employ model tests to carry out research [92]. However, the limitations of existing laboratory facilities (such as water depth and flow velocity) make it impractical to perform full-scale LWR model testing at reasonable scales. Due to the large spatial dimensions of the offshore platform and its riser system, the model obtained by using the conventional scale ratio (1/50–1/100) still exceeds the scale range of the current testing facilities. At present, both physical model tests and numerical simulation have their own advantages and disadvantages, and the hybrid model test method which combines the advantages of both is the most widely applied and recognized solution for deepwater platform model testing. One of the key considerations in implementing hybrid model testing is to design an equivalent truncated system that matches the characteristics of the full-scale system, allowing it to serve as a substitute for the full-scale system in existing size models [93]. Currently, there are many studies on the global response tests of the SCRs [94], but there is little experimental research on the global response of the LWRs. Since fatigue damage estimations for risers within the industry tend to be conservative, the STREAM Joint Industry Project (JIP) was the first in the industry to compile and analyze full-scale field data from five risers (4 SCRs and 1 SLWR) to provide measurement data for modeling risers and advance fatigue damage research [95].

Research on the global response of LWRs has primarily focused on VIV experimental studies, such as the VIV response under different staggered buoyancy config-

urations [6,37,87,96]. In 2011, Shell Oil Company ran advanced experiments to investigate the effects of buoyancy block spacing on the VIV response at the Marintek Ocean Laboratory in Norway. The riser VIV model adopted a 38 m long riser (made of glass fiber) with an outer diameter of 0.03 m and a wall thickness of 1.5 mm, where the buoyancy block is 0.41 m in length and 0.08 m in diameter (Table 1) [6]. In this experiment, the ratio of the buoyancy diameter to the riser diameter was set as 2.67. This non-integer ratio was set to prevent the vortex shedding frequency of the bare riser from being a multiple of that of the buoyancy blocks, which is very critical in the LWR design. If the higher harmonics of the buoyancy block vortex shedding frequency are equal to the shedding frequency of the bare riser, this enhances the global VIV response of the LWR.

Table 1. The dimensions of the LWRs.

Organization	Outer Diameter	Wall Thickness	Buoyancy Block's Length	Buoyancy Block's Diameter
Shell Oil Company's model	0.03 m	0.0015 m	0.41 m	0.08 m
NDP's model	0.03 m	0.0015 m	0.15 m	0.15 m

Subsequently, to achieve an optimal design and arrangement of staggered buoyancy blocks that minimizes the VIV response, the Norwegian Deepwater Program (NDP) performed hydrodynamic testing on SLWR models subjected the VIV in the MARINTEK offshore basin [96]. The same type of fiberglass riser employed in Shell's VIV model experiments for the bare riser was selected in this program. A key difference from Shell's VIV model experiments was that the buoyancy block diameter was significantly larger than that of the bare riser. The buoyancy blocks were measured 0.15 m in length and 0.15 m in diameter in this program (Table 1).

The model was tested by towing the riser with different speeds to simulate uniform flow (Figure 14). Unlike the use of fins to suppress VIV in previous studies [34], strakes were utilized in this experiment to mitigate vortex shedding, thereby reducing vortex-induced vibrations. This program found that a large diameter ratio between the buoyancy blocks and bare riser may result in a substantially lower shedding frequency for the buoyancy blocks, potentially exciting much lower structural modes.

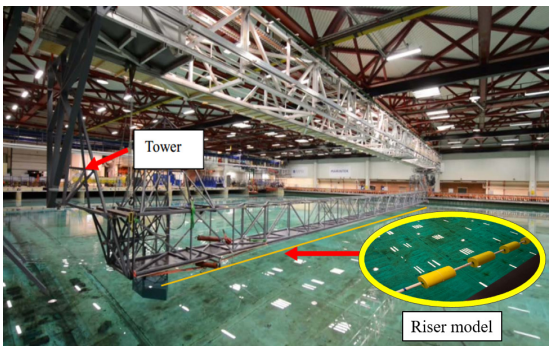

Figure 14. Test rig during testing—riser in water (adapted from [96]).

More and more new technologies have been applied in VIV experiments. Based on experimental models, Zhu et al. [91] conducted a study to investigate the VIV response of flexible LWRs filled with different fluid media. The experiment employed non-intrusive optical measurement techniques using a pair of high-speed cameras to simultaneously capture the IF and CF displacements with a sampling frequency of 100 Hz (Figure 15).

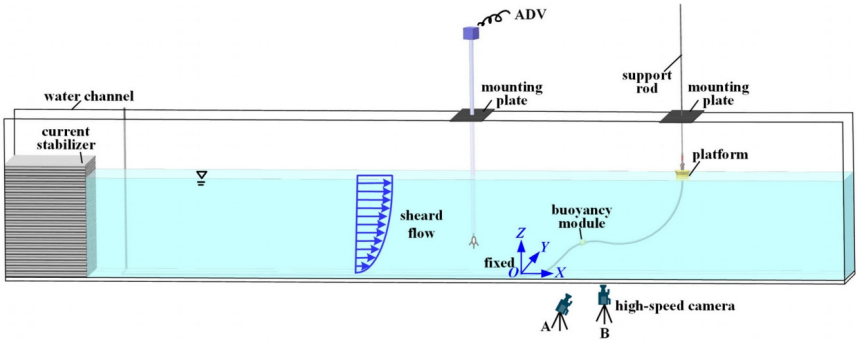

Figure 15. Schematic diagram of LWR's VIV test setup [91].

3.4. Abandonment and Recovery

In actual engineering projects, multiple offshore risers are typically installed on a floating platform. To improve construction progress and installation efficiency, a pre-lay approach is commonly adopted for the offshore laying and installation of marine risers. If the installation of the LWR is completed before the platform arrives, the LWR needs to be abandoned on the seabed and later recovered and reinstalled when the platform becomes available [97]. The LWR abandonment and recovery can be realized by controlling the tension and length of the A&R (Abandonment and Recovery) cable, as well as the position of the installation vessel. Many researchers have extensively studied the installation process of the SCRs [98–100], but there are fewer analyses on the installation process for LWRs, indicating a need for more comprehensive and in-depth research. There are numerous challenges that must be overcome during the abandonment, recovery, and tow transfer processes of LWR systems [101], which include determining the abandonment path for buoyancy blocks, applying tension to balance curve stability, ensuring the stability of the seabed's stagnation wave "hump", and applying stress at flexible joints, etc. Additionally, the recovery and transfer operations also face challenges related to gap monitoring between mooring lines and already installed risers.

According to the nonlinear large deformation beam theory, Wang et al. [102] divided the LWR transfer process into three stages (lowering stage, tension transfer stage, and recovery stage) to perform numerical analysis of the transfer process during the LWR installation. It was observed that the changes in the global riser configuration were very small compared to the local configurations near the pull-head and the TDP. In the same year, Wang et al. [97] pointed out that the LWR abandonment and recovery operations experienced a process with moving boundary conditions, making it difficult to determine the length of the riser suspended segment. Then, three different abandonment methods are employed for LWR installation operations: (1) maintain a constant top angle at the pull head during abandonment; (2) maintain a constant top tension at the pull head during abandonment; (3) maintain a constant configuration of the arch-shaped cross-section after the upper catenary portion of the SLWR contacts the seabed.

Given that hydrodynamic loads lead to continuous interaction between the riser and the seabed, the TDZ of the LWR is one of the fatigue hotspots [33]. Based on this, Wang et al. [50] developed an analytical model for the transfer process of the SLWR from the installation vessel to the production platform on an elastic seabed. This model facilitates the identification of an optimal installation path, ensuring the safety of the SLWR during the transfer process. Based on simulation-based design process, Jaewon et al. [23] utilized multi-body dynamics simulations to select effective parameters that influence the response and they leveraged open-source PIDO (Process Integration and Design Optimization) software to develop a dynamic simulation model to identify the optimal shape of an SLWR during installation. As depicted in Figure 16, Gu et al. [103] proposed an efficient computational program based on the principle of minimum potential energy, which was successfully applied to investigate the static tension effects during the installation process of the SLWR.

By considering various vessel movement speeds and cable recovery rates to execute the recovery methods, the recovery operations for an SLWR were assessed.

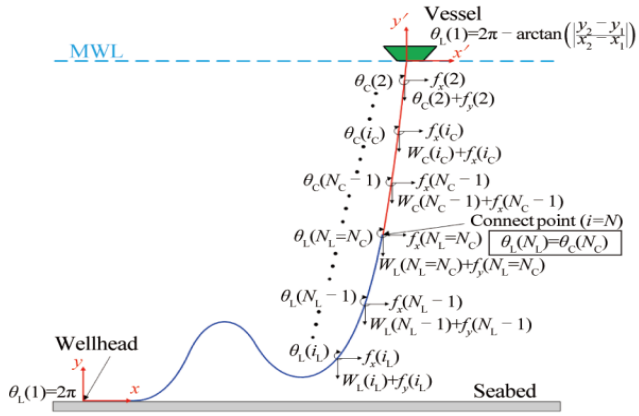

Figure 16. SLWR global coordinate system during abandonment and recovery [103].

4. Fatigue Damage of LWRs

The fatigue life of offshore risers is a critical aspect in the riser design process. Yang et al. [7] employed the finite element approach to carry out a dynamic stress analysis of the SLWR in the time domain, and systematically investigated the influence of hydrodynamic coefficients, structural damping, seabed stiffness, and floating structure motions on the fatigue damage of deepwater SLWR based on the S-N curve and Miner's linear cumulative damage rule. It was found that the motion characteristics of a floating structure have a significant impact on the fatigue damage of the SLWR. The research also indicated that increasing seabed stiffness by 15% reduces the minimum fatigue life in the TDZ from 158 years to 110 years from the base case. Based on Monte Carlo simulation with importance sampling (MCSIS), da Silva et al. [104] quantified the occurrence probability of failure modes and proposed a structural reliability fatigue solution to investigate the possibility of buoyancy length reduction in the LWR under fatigue failure modes (Figure 17). MCSIS is a numerical technique with variance reduction capability, and it is a method used to evaluate the probability of failure, requiring a relatively small number of samples (structural analyses) to obtain stable probability of failure (PF) results. This technique can be summarized by the following formula:

$$p_f = \frac{1}{N}\sum_{j=1}^{N}\left\{ I[G(x_j) \le 0]\frac{f_X(x_j)}{h_X(x_j)} \right\} \tag{32}$$

where $G(\boldsymbol{X})$ represents the failure function; $f_X(x)$ represents the joint probability density function of all random variables $\boldsymbol{X}$; $h_X(x)$ denotes the so-called sampling distribution. Based on the Palmgren–Miner's summation rule for fatigue damage associated with S–N curves, the fatigue design criterion can be expressed as follows:

$$\frac{T_{Ref}K_D}{\sum_{i=1}^{N} n_i(S_i)^m}\frac{\Delta}{SF} = \frac{T_{Ref}}{DT_{Ref}}\frac{\Delta}{SF} = \frac{FL}{SF} > T_{oper} \tag{33}$$

where K_D and m are the design S–N curve parameters; S_i denotes the stress cycles ranges identified in a reference period; Δ represents the allowable limit of accumulated fatigue damage; SF is a safety factor. In addition, the mean stress effect can be considered by means of the Gerber approach [105]. More detailed symbol explanations can be seen in [104].

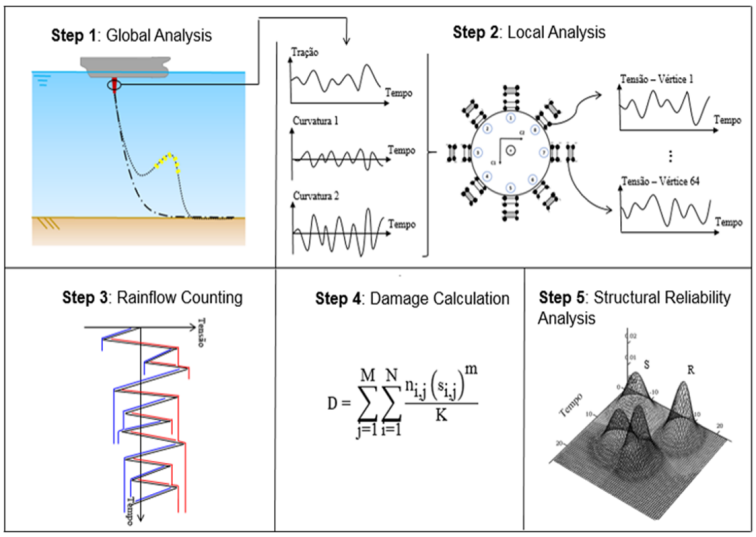

Figure 17. Fatigue calculation schematic sequence [104].

Hejazi et al. [106] employed extensive measured and hindcast metocean datasets in the fatigue design process of offshore risers. This research introduced a novel framework that leverages an "ANN-based technique" combined with the concept of a "representative (P50) year", which can make the direct application of large meteorological and oceanographic datasets estimate the riser fatigue life. Furthermore, the study proposed an innovative framework based on Monte Carlo methods to achieve more efficient long-term fatigue assessments of offshore risers. A fatigue monitoring approach for the SLWR based on a digital twin model was put forward by Lee et al. [107] to estimate the fatigue life of SLWRs in real-time. In this research, a machine learning algorithm was employed to estimate the 3D current distribution along the water column, which will be adopted as an additional load to refine the digital twin model. Based on a dual algorithm (DA), Chung et al. [108] put forward a novel structural health monitoring methodology for risers to accurately reproduce the movements and stresses along the whole lengths of the SCR and SLWR, with an error margin of approximately 5%, regardless of the riser's shape and material. This method not only can monitor the riser's condition, but also can assess the riser accumulated fatigue damage in real-time.

The buoyancy force provided by the buoyancy blocks makes the riser bulge and then produce a wave shape, which can effectively reduce the top tension of the riser and alleviate the coupling effect of the floating structure movement on the riser's TDZ, thus increasing the fatigue life of the area. In order to investigate the effect of buoyancy section number on the fatigue performance in the TDZ of the LWR, Ruan et al. [10] proposed a new concept of "multiple LWR", namely, LWR configuration based on multiple waveform serial arrangement (Figure 18).

Based on the improved slender rod theory, three riser configurations (catenary riser, LWR, multiple LWR) with different platform heave excitations and ocean currents were structured, and the corresponding dynamic response characteristics, excitation motion transfer paths, and fatigue damage hotspots were well compared. By constructing the lazy wave configuration, deepwater LWRs can attenuate the kinematic coupled response between the platform movement and riser's dynamic response in the TDZ, so as to optimize its anti-fatigue performance; compared to the LWR, multiple LWRs have some competitiveness in the anti-fatigue performance in the TDZ. Later, Ruan et al. [21] develop a systematic solution for the dynamic stress evaluation of flexible LWRs suffering from random wave and vessel motions, which can provide a good basis for fatigue analysis and damage assessment of LWRs.

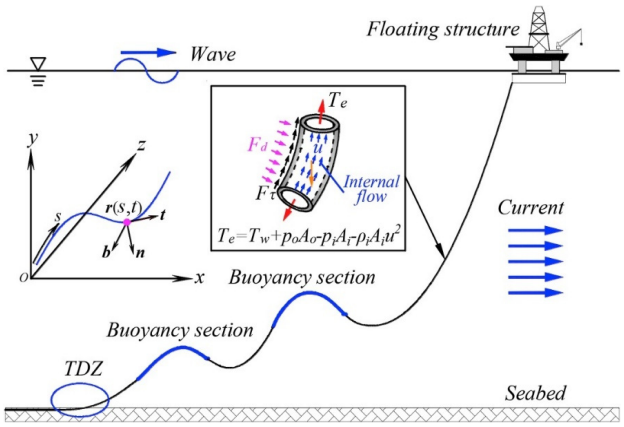

Figure 18. Schematic diagram of multiple LWR [10].

5. Structural Optimization of LWRs

The introduction of buoyancy blocks will increase the number of design parameters for the LWRs, making the optimization a pressing challenge. The unique structural form of LWRs also contributes to the configurational complexity, with different configurations varying significantly in terms of structural strength, mechanical performance, fatigue life, and economics. This brings significant uncertainty into the optimization design of LWRs. Given the numerous and interdependent design parameters, an increasing number of optimization algorithms have been applied in this field, achieving remarkable success. Based on genetic algorithm (GA), Tanaka et al. [30] took material and installation costs as the optimization goal to obtain an optimal LWR static configuration. Based on the given inner diameters and materials of the riser and buoyancy block, the optimizer was allowed to freely vary the number of riser segments, as well as the thickness, length, and buoyancy block diameter of each segment within user-defined ranges. Nevertheless, genetic algorithms have their limitations in this context. When dynamic and fatigue analyses are included, each evaluation of the objective function and constraints will take a longer time, potentially affecting the overall optimization efficiency. Furthermore, the optimized solution may be overly sensitive to small parameter changes, resulting in unrealistic configurations that become unfeasible due to manufacturing and installation tolerances and uncertainties.

De Pina et al. [31] employed a particle swarm optimization (PSO) algorithm to optimize the design of LWRs with the goal of minimizing cost, while considering requirements such as maximum equivalent stress, maximum total hanging angle, maximum tension, and minimum tension. This optimization process involved adjusting the length of each riser segment and the size of buoyancy materials. For specific optimization problems, the internal parameters in the PSO algorithm can significantly influence the optimization outcome. Aiming to identify the most cost-effective sizes, quantities, and positions of buoyancy blocks for lazy wave umbilical cables in installations, Yang et al. [109] proposed a multi-objective optimization method based on an approximation model for the dynamic installation of umbilical cables. The research took full account of the dynamic effects of environmental loads, resulting in safer and more accurate optimized results.

The optimization objective for LWRs is typically to achieve a cost-effective configuration while still being able to withstand extreme and fatigue loads, which leads to a balancing act between cost targets and multi-constraint engineering design problems. However, quantifying costs can be challenging due to factors such as material, installation, maintenance, and operation. Therefore, it is more appropriate to take objective functions based on structural criteria (e.g., strength, buckling, fatigue, and interference) during the design process. Ai et al. [17] achieved stress-based and fatigue-based objective optimizations in the distribution design of buoyancy blocks for the LWRs using genetic algorithm. It was noted that the definition of the objective function is not unique for critical design aspects. The distribution of buoyancy blocks is optimized to achieve an optimal configuration while minimizing stress, referred to as the stress objective. Therefore, the optimization problem

can be defined as finding the solution vector x that minimizes the objective function f(x) within the given variable limits and constraints:

$$\begin{cases} \text{minimize Damage}(x) \text{ or Stress}(x)\ x \in R^n \\ x_i^l \le x_i \le x_i^u, i = 1, \ldots, 4 \\ \text{limit } \alpha, Z_{\max} \text{and} Z_{\min} \end{cases} \tag{34}$$

where $x_i{}^l$ and $x_i{}^u$ represent the lower and upper limits of the ith design variable.

Based on index optimization techniques, Ogbeifun et al. [110] came up with a 2D tabular optimization method for LWRs. This method can simplify the multi-dimensional problem into a 2D format, which can significantly reduce the computational resources required. In this approach, design variables are assembled in pairs, and indexes are assigned to the resulting design points for each combination, finally the optimal design points are tracked through index matching by data sorting and intersection operation techniques. This technology is utilized to optimize the LWR hanging length and hang-off tension, buoyancy section length, buoyancy module thickness, etc. Most studies employ standard GA or PSO to address problems with continuous design variables. However, discrete variables are involved in the design process for LWRs, such as the number of buoyancy blocks, which standard algorithms are not sufficient to handle. Therefore, improved algorithms are required to effectively deal with both continuous and discrete variables. Yu et al. [111] setup a self-developed program to calculate steel double LWR dynamics in a fully coupled platform/mooring/riser system, taking each segment length and buoyancy block parameter as design variables, and adopting the maximum static stress, horizontal motion range, and maximum dynamic stress standard deviation as optimization objectives. An improved PSO was proposed to handle both continuous and discrete design variables to automatically seek out the optimal solution. Furthermore, Feedforward Neural Networks (FNNs) were embedded into the optimization algorithm to replace time-consuming numerical calculations. The results showed that the FNNs provide high accuracy with an error of no more than 6.34%, and all determination coefficients are about 0.95.

6. Conclusions

In this paper, the research on LWRs over the past two decades is reviewed, outlining the unique structure of LWRs, hydrodynamic loads, global responses, fatigue damage, and the current state of research and achievements in the structural configuration optimization. In terms of global responses, the global static/dynamic response, vortex-induced vibration, installation, transfer, repair and other technical means, and research results are introduced from three aspects: numerical simulation, theoretical method, and model experiment.

The research status and advantages/disadvantages of the 2D mechanical model and 3D mechanical model for the LWRs are systematically summarized and compared. When conditions permit, 3D modeling should be the goal, and nonlinear large deformation theory should be employed. When computational resources are sufficient, fully coupled solutions should be adopted, avoiding uncoupled solutions as they can lead to low accuracy, especially in deep water scenarios. In model experiments, due to the inability to support full-scale models, it is essential to ensure that boundary conditions are satisfied when conducting truncated experiments to improve the accuracy of the results.

In addressing fatigue damage and the structural optimization of the LWRs, it is crucial to keep up with advancements and effectively utilize various advanced algorithms for analysis, ultimately achieving complementary advantages. The optimization of LWR configurations should incorporate target functions based on structural standards (such as strength, buckling, fatigue, and interference) during the design process. There are few studies on the LWR global response model test and the hydrodynamic test of the buoyancy section, so more numerous and deeper studies should be carried out to support the accurate calculation of the hydrodynamic loads in the buoyancy section of the LWR.

Author Contributions: Conceptualization, W.R. and Y.B.; methodology, W.R. and Y.B.; validation, Y.B.; investigation, C.Z. and B.S.; resources, W.R. and B.S.; writing—original draft preparation, W.R., C.Z., H.Y., and Z.W.; writing—review and editing, W.R., C.Z., H.Y., and Z.W.; supervision, B.S.; funding acquisition, W.R. All authors have read and agreed to the published version of the manuscript.

Funding: This research was funded by the Natural Science Foundation of Zhejiang Province (Grant No. LY23E090004), the Fundamental Research Funds for the Provincial Universities of Zhejiang (Grant No. RF-A2022006), the Ningbo Natural Science Foundation (Grant No. 2021J039), and the National Natural Science Foundation of China (Grant No. 51909236).

Institutional Review Board Statement: Not applicable.

Informed Consent Statement: Not applicable.

Data Availability Statement: Data will be made available upon request.

Conflicts of Interest: The authors declare no conflicts of interest.

References

1. Guo, X.; Fan, N.; Liu, Y.; Liu, X.; Wang, Z.; Xie, X.; Jia, Y. Deep seabed mining: Frontiers in engineering geology and environment. *Int. J. Coal Sci. Technol.* **2023**, *10*, 23. [CrossRef]
2. Bai, Q.; Bai, Y. 1—Introduction. In *Subsea Pipeline Design, Analysis, and Installation*; Bai, Q., Bai, Y., Eds.; Gulf Professional Publishing: Oxford, UK, 2014; pp. 3–21. [CrossRef]
3. Ruan, W.; Nie, Q.; Han, X.; Li, J.; Bai, Y.; Fu, X. Accurate modeling and safety evaluation of dented pipeline with internal pressure based on reverse modeling technique. *Ships Offshore Struct.* **2024**, 1–11. [CrossRef]
4. Yue, B.; Campbell, M.; Walters, D.; Thompson, H.; Raghavan, K. Improved SCR Design for Dynamic Vessel Applications. In Proceedings of the ASME 2010 29th International Conference on Ocean, Offshore and Arctic Engineering, Shanghai, China, 6–11 June 2010; pp. 495–504. [CrossRef]
5. Orimolade, A.P.; Karunakaran, D.; Meling, T.S. Steel Lazy Wave Risers From Turret Moored FPSO for Deepwater Harsh Environment. In Proceedings of the ASME 2015 34th International Conference on Ocean, Offshore and Arctic Engineering, Newfoundland, Canada, 31 May–5 June 2015. [CrossRef]
6. Jhingran, V.; Zhang, H.; Lie, H.; Braaten, H.; Vandiver, J.K. Buoyancy Spacing Implications for Fatigue Damage due to Vortex-Induced Vibrations on a Steel Lazy Wave Riser (SLWR). In Proceedings of the Offshore Technology Conference, Houston, TX, USA, 30 April–3 May 2012. [CrossRef]
7. Yang, H.; Li, H. Sensitivity analysis of fatigue life prediction for deepwater steel lazy wave catenary risers. *Sci. China Technol. Sci.* **2011**, *54*, 1881–1887. [CrossRef]
8. Karunakaran, D.; Nordsve, N.; Olufsen, A. An Efficient Metal Riser Configuration for Ship and Semi Based Production Systems. In Proceedings of the Sixth International Offshore and Polar Engineering, Los Angeles, CA, USA, 26–31 May 1996; pp. 156–162.
9. Hu, B.; Wang, Z.; Du, H.; Carriveau, R.; Ting, D.S.K.; Xiong, W. Response characteristics of flexible risers in offshore compressed air energy storage systems. *J. Marine. Sci. Appl.* **2019**, *18*, 353–365. [CrossRef]
10. Ruan, W.; Shi, J.; Sun, B.; Qi, K. Study on fatigue damage optimization mechanism of deepwater lazy wave risers based on multiple waveform serial arrangement. *Ocean Eng.* **2021**, *228*, 108926. [CrossRef]
11. Wu, M.; Huang, K. The comparison of various SCR configurations for bow turret moored FPSO in West Africa. In Proceedings of the 17th International Offshore and Polar Engineering Conference (ISOPE 2007), Lisbon, Portugal, 1–6 July 2007. Available online: https://onepetro.org/ISOPEIOPEC/proceedings-abstract/ISOPE07/All-ISOPE07/ISOPE-I-07-054/11041 (accessed on 24 August 2024).
12. Ruan, W.; Liu, S.; Li, Y.; Bei, Y.; Yuan, S. Nonlinear Dynamic Analysis of Deepwater Steel Lazy Wave Riser Subjected to Imposed Top-End Excitations. In Proceedings of the 35th ASME International Conference on Ocean, Offshore and Arctic Engineering, Busan, Republic of Korea, 19–24 June 2016. [CrossRef]
13. Ruan, W.; Bai, Y.; Cheng, P. Static analysis of deepwater lazy-wave umbilical on elastic seabed. *Ocean Eng.* **2014**, *91*, 73–83. [CrossRef]
14. Ruan, W.; Shang, Z.; Wu, J. Effective static stress range estimation for deepwater steel lazy-wave riser with vessel slow drift motion. *Ships Offshore Struct.* **2019**, *14*, 899–909. [CrossRef]
15. Kim, S.; Kim, M.H. Dynamic behaviors of conventional SCR and lazy-wave SCR for FPSOs in deepwater. *Ocean Eng.* **2015**, *106*, 396–414. [CrossRef]
16. Felisita, A.; Gudmestad, O.T.; Karunakaran, D.; Martinsen, L.O. Review of Steel lazy wave riser concepts for the North Sea. *J. Offshore Mech. Arct. Eng. Trans. ASME* **2017**, *139*, 15. [CrossRef]
17. Ai, S.M.; Xu, Y.; Kang, Z.; Yan, F. Performance comparison of stress-objective and fatigue-objective optimisation for steel lazy wave risers. *Ships Offshore Struct.* **2019**, *14*, 534–544. [CrossRef]
18. Wang, J.; Duan, M.; He, T.; Jing, C. Numerical solutions for nonlinear large deformation behaviour of deepwater steel lazy-wave riser. *Ships Offshore Struct.* **2014**, *9*, 655–668. [CrossRef]

19. Wang, J.; Duan, M. A nonlinear model for deepwater steel lazy-wave riser configuration with ocean current and internal flow. *Ocean Eng.* **2015**, *94*, 155–162. [CrossRef]
20. Yang, Z.; Yan, J.; Sævik, S.; Zhen, L.; Ye, N.; Chen, J.; Yue, Q. Multi-Objective Optimization Design of Flexible Risers Based on Bi-Scale Response Surface Models. In Proceedings of the ASME 2018 37th International Conference on Ocean, Offshore and Arctic Engineering. Volume 5: Pipelines, Risers, and Subsea Systems, Madrid, Spain, 17–22 June 2018. [CrossRef]
21. Cheng, Y.; Tang, L.Y.; Fan, T.H. Dynamic analysis of deepwater steel lazy wave riser with internal flow and seabed interaction using a nonlinear finite element method. *Ocean Eng.* **2020**, *209*, 107498. [CrossRef]
22. Ruan, W.; Nie, Q.L.; Lu, Y.T.; Chen, M.Y.; Liu, D.H.; Sun, B. A global-local approach for dynamic stress evaluation of lazy wave flexible risers subjected to random wave and vessel motion. *Ships Offshore Struct.* **2023**, *18*, 810–826. [CrossRef]
23. Oh, J.; Jung, D.; Kim, H.; Min, C.; Cho, S. A study on the simulation-based installation shape design method of steel lazy wave riser (SLWR) in ultra deepwater depth. *Ocean Eng.* **2020**, *197*, 106902. [CrossRef]
24. Ruan, W.; Bai, Y.; Yuan, S. Dynamic analysis of unbonded flexible pipe with bend stiffener constraint and bending hysteretic behavior. *Ocean Eng.* **2017**, *130*, 583–596. [CrossRef]
25. de Sousa, J.R.M.; Sousa, F.J.M.; Siqueira, M.Q.; Sagrilo, L.V.S.; de Lemos, C.A.D. A theoretical approach to predict the fatigue life of flexible pipes. *J. Appl. Math.* **2012**, *8*, 983819. [CrossRef]
26. Zhao, B. Fatigue Analysis of Flexible Riser-Effect of Mean Stress Correction Procedures. Master's Thesis, Institutt for Marin Teknikk, Trondheim, Norway, 2013. Available online: https://api.semanticscholar.org/CorpusID:107448295 (accessed on 24 August 2024).
27. Yin, D.; Lie, H.; Wu, J. Structural and hydrodynamic aspects of steel lazy wave riser in deepwater. *J. Offshore Mech. Arct. Eng. Trans. ASME* **2020**, *142*, 020801. [CrossRef]
28. Shanharan, R.; Anaturk, A.; Howells, H.; Lopes, M. Feasibility of Steel Lazy Wave Risers in the North Sea. In Proceeding of the MCD Deepwater Development, Addison-Wesley, Amsterdam, Netherlands, 3–5 April 2017. Available online: https://mcedd.com/wp-content/uploads/2017/Proceedings/14/MCEDD%202017%20Feasibility%20of%20Steel%20Lazy%20Wave%20Risers%20in%20the%20North%20Sea%20(Final).pdf (accessed on 24 August 2024).
29. Amaechi, C.V.; Wang, F.C.; Ye, J.Q. Investigation on Hydrodynamic Characteristics, Wave-Current Interaction and Sensitivity Analysis of Submarine Hoses Attached to a CALM Buoy. *J. Marine Sci. Eng.* **2022**, *10*, 120. [CrossRef]
30. Tanaka, R.L.; de Arruda Martins, C. A Genetic Algorithm Approach to Steel Riser Optimization. In Proceedings of the 25th International Conference on Offshore Mechanics and Arctic Engineering. Volume 1: Offshore Technology; Offshore Wind Energy; Ocean Research Technology; LNG Specialty Symposium, Hamburg, Germany, 4–9 June 2006; pp. 271–277. [CrossRef]
31. de Pina, A.A.; Albrecht, C.H.; de Lima, B.S.L.P.; Jacob, B.P. Tailoring the particle swarm optimization algorithm for the design of offshore oil production risers. *Optim. Eng.* **2011**, *12*, 215–235. [CrossRef]
32. Trapper, P.A. Feasible numerical analysis of steel lazy-wave riser. *Ocean Eng.* **2020**, *195*, 106643. [CrossRef]
33. Hou, Z.; Gaudin, C.; Sahdi, F.; Randolph, M. Centrifuge modelling of whole-life pipe-soil interaction in clay with different overconsolidation ratios. *Geotechnique* **2022**, *73*, 1056–1070. [CrossRef]
34. Ertekin, R.C.; Rodenbusch, G. Wave, current and wind loads. In *Springer Handbook of Ocean Engineering*; Dhanak, M.R., Xiros, N.I., Eds.; Springer International Publishing: Cham, Switzerland, 2016; pp. 787–818. [CrossRef]
35. Sarpkaya, T.S.; Isaacson, M.; Wehausen, J.V. Mechanics of wave forces on offshore structures. *J. Appl. Mech.* **1982**, *49*, 466–467. [CrossRef]
36. Sarpkaya, T.S. Wave Forces on Offshore Structures. Cambridge University Press: Cambridge, UK, 2010. [CrossRef]
37. Rao, Z.; Vandiver, J.K.; Jhingran, V. Vortex induced vibration excitation competition between bare and buoyant segments of flexible cylinders. *Ocean Eng.* **2015**, *94*, 186–198. [CrossRef]
38. Zhu, H.; Zhao, H.; Srinil, N. Experimental investigation on vortex-induced vibration and solid-structure impact of a near-bottom horizontal flexible pipeline in oblique shear flow. *J. Fluids Struct.* **2021**, *106*, 103356. [CrossRef]
39. El-Reedy, M.A. (Ed.) 4—Offshore structures design. In *Marine Structural Design Calculations*; Butterworth-Heinemann: Oxford, UK, 2015; pp. 85–187. [CrossRef]
40. Chanson, H. *Applied Hydrodynamics: An Introduction to Ideal and Real Fluid Flowsi*, 1st ed.; CRC Press: Boca Raton, FL, USA, 2009. [CrossRef]
41. Papillon, L.; Costello, R.; Ringwood, J.V. Boundary element and integral methods in potential flow theory: A review with a focus on wave energy applications. *J. Ocean. Eng. Mar. Energy* **2020**, *6*, 303–337. [CrossRef]
42. Xu, P.; Gong, S. Pipelay parametric investigation of pipeline dynamic behaviours for deepwater S-lay operation. *Ships Offshore Struct.* **2020**, *15*, 1141–1155. [CrossRef]
43. Xu, P.; Du, Z.; Huang, F.; Javanmardi, A. Numerical simulation of deepwater S-lay and J-lay pipeline using vector form intrinsic finite element method. *Ocean Eng.* **2021**, *234*, 109039. [CrossRef]
44. Orcina. *Orcaflex Manual*; Version 9.8a; Orcina Ltd.: Ulverton, Cumbria, UK, 2014. Available online: https://www.orcina.com/webhelp/OrcaFlex/Default.htm (accessed on 16 February 2020).
45. Morison, J.R.; Johnson, J.W.; Schaaf, S.A. The force exerted by surface waves on piles. *J. Pet. Technol.* **1950**, *2*, 149–154. [CrossRef]
46. Ruan, W.; Dai, W.; Wu, J. Study on motion transfer rule and extreme dynamic response of SCR's top-end heave excitation. *J. Mar. Eng. Technol.* **2021**, *20*, 186–199. [CrossRef]

47. Wang, J.; Duan, M.; He, R. A nonlinear dynamic model for 2D deepwater steel lazy-wave riser subjected to top-end imposed excitations. *Ships Offshore Struct.* **2018**, *13*, 330–342. [CrossRef]
48. Li, X.; Guo, X.; Guo, H. Vector form intrinsic finite element method for nonlinear analysis of three-dimensional marine risers. *Ocean Eng.* **2018**, *161*, 257–267. [CrossRef]
49. Hasanvand, E.; Edalat, P. Evaluation of the safe and failure zones of mooring and riser systems in a CALM oil terminal. *J. Mar. Sci. Appl.* **2021**, *20*, 751–766. [CrossRef]
50. Wang, Y.; Duan, M.; Gu, J. Analytical model for transfer process of deepwater steel lazy-wave riser on elastic seabed. *J. Mar. Sci. Technol.* **2019**, *24*, 123–133. [CrossRef]
51. Guarracino, F.; Mallardo, V. A refined analytical analysis of submerged pipelines in seabed laying. *Appl. Ocean Res.* **1999**, *21*, 281–293. [CrossRef]
52. Sparks, C.P. *Fundamentals of Marine Riser Mechanics: Basic Principles and Simplified Analyses*; Penn Well: Tulsa, OK, USA, 2007. Available online: https://books.google.com.hk/books?id=z0urYVzcFLUC (accessed on 28 August 2024).
53. Irani, M.B.; Modi, V.J.; Welt, F. Riser dynamics with internal flow and nutation damping. In Proceedings of the Sixth International Offshore Mechanics and Arctic Engineering Symposium, Houston, TX, USA, 1 March 1987; Volume 3, pp. 119–125.
54. Chucheepsakul, S.; Huang, T. Influence of Transported Mass On the Equilibrium Configuration of Risers. In Proceedings of the Fourth International Offshore and Polar Engineering Conference, Osaka, Japan, 10 April 1994; ISOPE-I-94-124. Available online: https://onepetro.org/ISOPEIOPEC/proceedings-abstract/ISOPE94/All-ISOPE94/26093 (accessed on 28 August 2024).
55. Jeong, H.; Jang, B.S.; Kim, J.D.; Park, G.; Choi, J.; Lee, D. A study on effects of slug flow on dynamic response and fatigue damage of risers. *Ocean Eng.* **2020**, *217*, 107965. [CrossRef]
56. Cabrera-Miranda, J.M.; Paik, J.K. Two-phase flow induced vibrations in a marine riser conveying a fluid with rectangular pulse train mass. *Ocean Eng.* **2019**, *174*, 71–83. [CrossRef]
57. Zhang, C.; Kang, Z.; Ma, G.; Xu, X. Mechanical modeling of deepwater flexible structures with large deformation based on absolute nodal coordinate formulation. *J. Mar. Sci. Technol.* **2019**, *24*, 1241–1255. [CrossRef]
58. Wang, C.; Liu, J.; Li, B.; Huang, W. The absolute nodal coordinate formulation in the analysis of offshore floating operations, Part II: Code validation and case study. *Ocean Eng.* **2023**, *281*, 114650. [CrossRef]
59. Jamaludin, F.E.; Koto, J. Catenary offset buoyant riser assembly for Malaysian deepwater. *Sci. Eng.* **2017**, *12*, 9–14. Available online: https://isomase.org/JSOse/Vol.12%20Dec%202017/12-2.pdf (accessed on 28 August 2024).
60. Karunakaran, D.N.; Baarholm, R. COBRA: An Uncoupled Riser System for Ultradeep Water in Harsh Environment. In Proceedings of the Offshore Technology Conference, Houston, TX, USA, 6–9 May 2013. OTC-23986-MS. [CrossRef]
61. Karunakaran, D.; Aasen, H.; Baarholm, R. New Un-coupled Deepwater Riser Concept for Harsh Environment–Catenary Offset Buoyant Riser Assembly (COBRA). In Proceedings of the Deepwater Offshore Technology Conference, New Orleans, LA, USA, 1 October 2011; pp. 11–13.
62. Nurwanto, T.; Karunakaran, D.; Franciss, R. COBRA Riser Concept for Ultra Deepwater Condition. In Proceedings of the ASME 2013 32nd International Conference on Ocean, Offshore and Arctic Engineering, Nantes, France, 9–14 June 2013. V04BT04A030. [CrossRef]
63. Ormberg, H.; Larsen, K. Coupled analysis of floater motion and mooring dynamics for a turret-moored ship. *Appl. Ocean. Res.* **1998**, *20*, 55–67. [CrossRef]
64. Ormberg, H.; Fylling, I.J.; Larsen, K.; Sødahl, N. Coupled Analysis of Vessel Motions and Mooring and Riser System Dynamics. In Proceedings of the International Conference on Offshore Mechanics and Arctic Engineering, Yokohama, Japan, 13–17 April 1997; pp. 91–100. Available online: https://jglobal.jst.go.jp/en/detail?JGLOBAL_ID=200902146948838040#:~:text=Coupled%20an (accessed on 2 September 2024).
65. Nordgren, R.P. On Computation of the motion of elastic rods. *J. Appl. Mech.* **1974**, *41*, 777–780. [CrossRef]
66. Garrett, D.L. Dynamic analysis of slender rods. *J. Energy Res. Technol.* **1982**, *104*, 302–306. [CrossRef]
67. Ma, W.; Lee, M.; Zou, J.; Huang, E.W. Deepwater Nonlinear Coupled Analysis Tool. In Proceedings of the Offshore Technology Conference, Houston, TX, USA, 1 May 2000. [CrossRef]
68. Low, Y.M.; Langley, R.S. Time and frequency domain coupled analysis of deepwater floating production systems. *Appl. Ocean Res.* **2006**, *28*, 371–385. [CrossRef]
69. Gu, H.; Guo, H.; Li, X.; Li, F.; Liu, Z.; Cui, P. Three-dimensional dynamic analysis of deep-water steel steep wave riser considering internal solitary wave. *J. Mar. Sci. Technolo.* **2022**, *27*, 452–466. [CrossRef]
70. Paulling, J.R.; Webster, W.C. A Consistent, Large-amplitude Analysis of the Coupled Response of a TLP and Tendon System. In Proceedings of the Fifth International Symposium on Offshore Mechanics and Arctic Engineering, Tokyo, Japan, 13–18 April 1986; American Society of Mechanical Engineers: New York, NY, USA; pp. 126–133. Available online: https://pascal-francis.inist.fr/vibad/index.php?action=getRecordDetail&idt=7963711 (accessed on 2 September 2024).
71. Ran, Z.H. Coupled Dynamic Analysis of Floating Structures in Waves and Currents. Ph.D. Dissertation, Texas A&M University, College Station, TX, USA, 2000. Available online: https://www.proquest.com/openview/65c0d6db18d616309960b1ba01b72e1e/1?pq-origsite=gscholar&cbl=18750&diss=y (accessed on 2 September 2024).
72. Kim, Y.B. Dynamic Analysis of Multiple-Body Floating Platforms Coupled with Mooring Lines and Risers. Ph.D. Dissertation, Texas A&M University, College Station, TX, USA, 2003. Available online: https://oaktrust.library.tamu.edu/server/api/core/bitstreams/2efba84c-2509-40bd-8624-97b9eae21ed3/content (accessed on 2 September 2024).

73. Ryu, S. Hull/Mooring/Riser Coupled Motion Simulations of Thruster-Assisted Moored Platforms. Ph.D. Dissertation, Texas A&M University, College Station, TX, USA, 2005. Available online: https://www.proquest.com/openview/b1cb14c54820f776e06256136c6151ea/1?pq-origsite=gscholar&cbl=18750&diss=y (accessed on 2 September 2024).
74. Tahar, A.; Kim, M.H. Hull/mooring/riser coupled dynamic analysis and sensitivity study of a tanker-based FPSO. *Appl. Ocean Res.* **2003**, *25*, 367–382. [CrossRef]
75. Tahar, A.; Kim, M.H. Coupled-dynamic analysis of floating structures with polyester mooring lines. *Ocean Eng.* **2008**, *35*, 1676–1685. [CrossRef]
76. Li, F.; Guo, H.; Gu, H.; Liu, Z.; Li, X. Deformation and stress analysis of the deepwater steel lazy wave riser subjected to internal solitary waves. *J. Ocean Univ. China.* **2023**, *22*, 377–392. [CrossRef]
77. Ruan, W.; Chen, M.; Nie, Q.; Xu, P.; Li, J.; Wang, X. Dynamic response of steel lazy wave riser considering the excitation of internal solitary wave and ocean currents. *Ocean Eng.* **2024**, *294*, 116708. [CrossRef]
78. Yu, Y.; Zhao, M.; Li, Z.; Yu, J.; Liu, C.; Xu, L. Comparative dynamic analysis of SCR and LWR in the coupled platform-mooring-riser system under internal solitary wave conditions. *Ocean Eng.* **2023**, *267*, 113215. [CrossRef]
79. Williamson, C.H. Vortex dynamics in the cylinder wake. *Annu. Rev. Fluid Mech.* **1996**, *28*, 477–539. [CrossRef]
80. Buresti, G. Vortex shedding from bluff bodies. In *Wind Effects on Buildings and Structures*; Riera, J.D., Davenport, A.G., Eds.; Balkema Publishers: Rotterdam, The Netherlands, 1998; pp. 61–95. Available online: https://www.researchgate.net/publication/321367112 (accessed on 4 September 2024).
81. Perry, A.E.; Chong, M.S.; Lim, T.T. The vortex-shedding process behind two-dimensional bluff bodies. *J. Fluid Mech.* **1982**, *116*, 77–90. [CrossRef]
82. Yin, D. Heave motion induced vortex-induced vibrations of a full-scale steel lazy wave riser. *ASME J. Offshore Mech. Arct. Eng. Trans.* **2022**, *144*, 041905. [CrossRef]
83. Yin, D. On Vessel Motion Induced Vortex-Induced Vibrations of a Steel Lazy Wave Riser. In Proceedings of the ASME 2021 40th International Conference on Ocean, Offshore and Arctic Engineering; Volume 4: Pipelines, Risers, and Subsea Systems, Online, 21–30 June 2021. [CrossRef]
84. Jang, H.; Kim, J.W. Numerical Investigation for Vortex-Induced Vibrations of Steel-Lazy-Wave-Risers: Part II—CFD Study on Long Flexible Riser. In Proceedings of the ASME 2019 38th International Conference on Ocean, Offshore and Arctic Engineering, Glasgow, Scotland, UK, 9–14 June 2019. [CrossRef]
85. Constantinides, Y.; Zhang, M. VIV Assessment of Deepwater Lazy-Wave Risers. In Proceedings of the ASME 2014 33rd International Conference on Ocean, Offshore and Arctic Engineering, San Francisco, CA, USA, 8–13 June 2014. [CrossRef]
86. Wang, J.; Fu, S.; Baarholm, R.; Wu, J.; Larsen, C.M. Out-of-plane vortex-induced vibration of a steel catenary riser caused by vessel motions. *Ocean Eng.* **2015**, *109*, 389–400. [CrossRef]
87. Rao, Z.; Vandiver, J.K.; Jhingran, V. VIV Excitation Competition Between Bare and Buoyant Segments of Flexible Cylinders. In Proceedings of the ASME 2013 32nd International Conference on Ocean, Offshore and Arctic Engineering, Nantes, France, 9–14 June 2013. [CrossRef]
88. Li, A.; Wu, B.; Fan, D. Vortex-induced vibration of risers with staggered buoyancy modules of small aspect ratio. *Appl. Ocean Res.* **2022**, *120*, 103014. [CrossRef]
89. Bordalo, S.N.; Morooka, C.K. Slug flow induced oscillations on subsea petroleum pipelines. *J. Pet. Sci. Eng.* **2018**, *165*, 535–549. [CrossRef]
90. Bossio, V.B.M.; Blanco, A.A.J.; Casanova, M.E.L. Numerical modeling of the dynamical interaction between slug flow and vortex induced vibration in horizontal submarine pipelines. *J. Offshore Mech. Arct. Eng.* **2014**, *136*, 041803. [CrossRef]
91. Zhu, H.; Liu, W.; Gao, Y.; Deng, K.R.; Zhou, T.M. Experimental investigation on the vortex-induced vibration response of a lazy-wave flexible riser filled with different fluid media. *Phys. Fluids* **2024**, *36*, 037106. [CrossRef]
92. Guo, L.; Pang, X.; Kuang, J.; Liu, S.; Nie, Y. Experimental study on coupling dynamics of a high dimensional nonlinear riser structure and floating platform by truncated equivalent method. *Expe. Tech.* **2024**, *48*, 523–535. [CrossRef]
93. Kim, M.H.; Koo, B.J.; Mercier, R.M.; Ward, E.G. Vessel/mooring/riser coupled dynamic analysis of a turret-moored FPSO compared with OTRC experiment. *Ocean Eng.* **2005**, *32*, 1780–1802. [CrossRef]
94. Bridge, C.; Howells, H.; Toy, N.; Parke, G.A.R.; Woods, R. Full-scale model tests of a steel catenary riser. *WIT Trans. Built Environ.* **2003**, *71*, 107–116. Available online: https://www.witpress.com/Secure/elibrary/papers/FSI03/FSI03011FU.pdf (accessed on 5 September 2024).
95. Deka, D.; Chandra, Y.; Campbell, M.; Santala, M.; Constantinides, Y.; Jin, J.; Darilmaz, I.; Nadathur, R.; Yiu, F. STREAM JIP–Insights into Steel Catenary Riser Response Using Measured Data. In Proceedings of the Offshore Technology Conference, Houston, TX, USA, 6–9 May 2019. Available online: https://onepetro.org/OTCONF/proceedings-abstract/19OTC/2-19OTC/D021S018R005/180663 (accessed on 5 September 2024).
96. Wu, J.; Lie, H.; Constantinides, Y.; Baarholm, R.J. NDP Riser VIV Model Test With Staggered Buoyancy Elements. In Proceedings of the ASME 2016 35th International Conference on Ocean, Offshore and Arctic Engineering. Volume 2: CFD and VIV, Busan, Republic of Korea, 19–24 June 2016. [CrossRef]
97. Wang, J.; Duan, M.; Luo, J. Mathematical model of steel lazy-wave riser abandonment and recovery in deepwater. *Mar. Struct.* **2015**, *41*, 127–153. [CrossRef]

98. Du, D.; Acevedo, V.A.; Hamadi, R.; Parikh, S. Static and dynamic mechanism of an SCR clamp system in deep water installation. In Proceedings of the 27th International Ocean and Polar Engineering Conference, San Francisco, CA, USA, 25–30 June 2017. Available online: https://onepetro.org/ISOPEIOPEC/proceedings-abstract/ISOPE17/All-ISOPE17/ISOPE-I-17-496/18122 (accessed on 5 September 2024).
99. Wang, H.; He, N.; Xu, F.; Cheng, Y. The Development and Installation of the SCR Pull-In System for Lingshui 17-2 Project. In Proceedings of the 32nd International Ocean and Polar Engineering Conference, Shanghai, China, 5 June 2022. Available online: https://onepetro.org/ISOPEIOPEC/proceedings-abstract/ISOPE22/All-ISOPE22/ISOPE-I-22-187/493786 (accessed on 5 September 2024).
100. Wever, R.; Hendriks, P. Deepwater SCR Installation with the HLV Thialf. In Proceedings of the ASME 2009 28th International Conference on Ocean, Offshore and Arctic Engineering. Volume 3: Pipeline and Riser Technology, Honolulu, HI, USA, 31 May 2009; pp. 787–795. [CrossRef]
101. Thomas, B.; Benirschke, A.; Sarkar, T. Parque das Conchas (BC-10) Steel Lazy Wave Riser Installation: Pre-Abandonment, Recovery and Transfer Challenges. In Proceedings of the Offshore Technology Conference 2010, Houston, TX, USA, 3–6 May 2010; p. OTC-20605-MS. [CrossRef]
102. Wang, J.; Duan, M.; Wang, Y.; Li, X.; Luo, J. A nonlinear mechanical model for deepwater steel lazy-wave riser transfer process during installation. *Appl. Ocean Res.* **2015**, *50*, 217–226. [CrossRef]
103. Gu, J.; Huang, J.; Gao, L.; Chen, L.; Jia, J.; Wang, S. Abandonment and Recovery Operation of Steel Lazy-Wave Riser in Deep-water by Controlled Vessel and Cable Velocity Rate. *China Ocean Eng.* **2023**, *37*, 29–41. [CrossRef]
104. da Silva, V.R.M.; Sagrilo, L.V.S.; Vignoles, M.A. Lazy-wave buoyancy length reduction based on fatigue reliability analysis. *ASME J. Offshore Mech. Arct. Eng. Trans.* **2018**, *140*, 031602. [CrossRef]
105. Almar-Næss, A. *Fatigue Handbook: Offshore Steel Structures*, 1st ed.; Tapir Academic Press: Trondheim, Norway, 1999.
106. Hejazi, R.; Grime, A.; Randolph, M.; Efthymiou, M. An efficient probabilistic framework for the long-term fatigue assessment of large diameter steel risers. *Appl. Ocean Res.* **2022**, *118*, 102941. [CrossRef]
107. Lee, Y.; Jin, C.; Kim, M.; Xu, W. Digital twin approach with minimal sensors for Riser's fatigue-damage estimation. *Int. J. Nav. Archit. Ocean Eng.* **2024**, *16*, 100603. [CrossRef]
108. Chung, W.; Jin, C.; Kim, M. Dual-algorithm hybrid method for riser structural health monitoring using the fewest sensors. *J. Mar. Sci. Eng.* **2022**, *10*, 1994. [CrossRef]
109. Yang, H.; Wang, A.; Li, H. Multi-objective optimization for deepwater dynamic umbilical installation analysis. *Sci. China Phys. Mech. Astron.* **2012**, *55*, 1445–1453. [CrossRef]
110. Ogbeifun, A.; Oterkus, S.; Race, J.; Naik, H.; Moorthy, D.; Bhowmik, S.; Ingram, J. A tabular optimisation technique for steel lazy wave riser. *IOP Conf. Ser. Mater. Sci. Eng.* **2021**, *1052*, 012022. [CrossRef]
111. Yu, Y.; Zhao, M.; Zhang, B.; Jin, Z.; Su, Y.; Tian, H.; Pang, H. Configuration design of a steel double lazy wave riser based on metamodel-assisted metaheuristic algorithms. *Appl. Ocean Res.* **2024**, *151*, 104159. [CrossRef]